RRA-T7909
31 October 1979

RRA RADIATION RESEARCH ASSOCIATES
Fort Worth, Texas

CALCULATION OF TIME DEPENDENT LIGHT TRANSMISSION TO A SATELLITE FROM A POINT ISOTROPIC SOURCE EMBEDDED IN A CLOUD

D. G. Collins

TECHNICAL REPORT
PREPARED UNDER
Contract No. 13-1370

Prepared for
Sandia Laboratories
Albuquerque, New Mexico 87115

Unclassified

SECURITY CLASSIFICATION OF THIS PAGE (When Data Entered)

REPORT DOCUMENTATION PAGE

READ INSTRUCTIONS BEFORE COMPLETING FORM

1. REPORT NUMBER: RRA-T7909	2. GOVT ACCESSION NO.
3. RECIPIENT'S CATALOG NUMBER	
4. TITLE (and Subtitle): CALCULATIONS OF TIME DEPENDENT LIGHT TRANSMISSION TO A SATELLITE FROM A POINT ISOTROPIC SOURCE EMBEDDED IN A CLOUD	5. TYPE OF REPORT & PERIOD COVERED: FINAL
	6. PERFORMING ORG. REPORT NUMBER: RRA-T7909
7. AUTHOR(s): Dave G. Collins	8. CONTRACT OR GRANT NUMBER(s): 13-1370
9. PERFORMING ORGANIZATION NAME AND ADDRESS: Radiation Research Associates, Inc. 3550 Hulen Street Fort Worth, TX 76107	10. PROGRAM ELEMENT, PROJECT, TASK AREA & WORK UNIT NUMBERS
11. CONTROLLING OFFICE NAME AND ADDRESS: Sandia Laboratories Albuquerque, NM 87115	12. REPORT DATE: 31 October 1979 13. NUMBER OF PAGES: 42
14. MONITORING AGENCY NAME & ADDRESS (if different from Controlling Office)	15. SECURITY CLASS. (of this report): Unclassified 15a. DECLASSIFICATION/DOWNGRADING SCHEDULE

16. DISTRIBUTION STATEMENT (of this Report)

APPROVED FOR PUBLIC RELEASE: DISTRIBUTION IS UNLIMITED
per Sandia Monitor 4/15/94

17. DISTRIBUTION STATEMENT (of the abstract entered in Block 20, if different from Report)

18. SUPPLEMENTARY NOTES

19. KEY WORDS (Continue on reverse side if necessary and identify by block number)

Light Scattering
Clouds
Pulse Stretching

20. ABSTRACT (Continue on reverse side if necessary and identify by block number)

Calculations of the time distributions for narrow-beam sources and receivers were utilized in an integration procedure to predict the time distribution of a signal received by a synchronous satellite due to a point isotropic source located beneath a dome shaped cloud. This time distribution is compared with a POLOE Monte Carlo calculation of the time dependent signal at a synchronous satellite for a point isotropic source within an infinite cloud layer. The comparisons are favorable for times beyond approximately

DD FORM 1 JAN 73 1473 EDITION OF 1 NOV 65 IS OBSOLETE

Unclassified

SECURITY CLASSIFICATION OF THIS PAGE (When Data Entered)

0.2 microseconds. At earlier times the time distribution based upon the narrow-beam results overpredicts the POLOE results by almost two orders of magnitude. It is thought that the simplyfing assumption made in order to develop the methods of integrating the narrow-beam source may well have caused the disagreement during early times.

TABLE OF CONTENTS

LIST OF FIGURES

LISTS OF TABLES

I. INTRODUCTION

The time delays attributed to light scattering within clouds have been determined to range from a few microseconds to several microseconds for cases where the initial signal is a point source beneath a cloud and the observation is from a point far enough above the cloud that a sizable portion of the scattering volume is within the receiver field-of-view, Ref. 1. However, time delays observed with a collimated receiver due to a laser pulse propagating within a cloud have been on the order of a few nanoseconds even when both the laser beam and the receiver axis were scanned off the source-receiver axis, Ref. 2. The purpose of this study is to determine whether these two significantly different time delays are inconsistant or whether the differences in the sources, receivers and geometric models account for the differences in the time delays.

The approach that has been taken to answer the above question is to utilize the time dependent data computed for the laser source to develop the time dependent transmission for a point isotropic source then to integrate the transmission developed for the isotropic source over the upper surface of a cloud to predict the time dependent signal at a satellite receiver positioned above the cloud. This time dependent receiver response would then be compared with the time dependent receiver response computed with the POLOE program for an isotropic source positioned beneath a cloud. This comparison should indicate whether the time responses computed for the laser pulse stretching and time delay study (Ref. 2) are inconsistant with the time delays determined for a point source beneath a cloud.

II. DEVELOPMENT OF TIME DEPENDENT TRANSMISSION DATA

During a previous study of the time delay and smearing of laser pulses propagating within a cloudy atmosphere calculations were made to determine the time dependent response of a collimated receiver for a 532 nanometer wavelength pulsed laser located 765 meters from the receiver where both the laser and the receiver were engulfed within a cloud. These data were generated in an attempt to model the atmospheric conditions and the experimental setup of Project CLIPS (Cloud-Induced Pulse Stretching) conducted by Sandia Laboratories during tests conducted in the Hawaiian Islands during the Fall of 1978. Fifty percent or more of the calculations were made for atmospheric conditions that produced a source-receiver optical separation distance of 14.7. Calculations of the time dependant receiver responses were made for both the laser source and the collimated receiver scanned at various angles off the source-receiver axis up to 10 degrees. Time delays in the order of a few nanoseconds depending upon the particular orientations of the source beam and collimated receiver axis were in general in good agreement with the measured time delays. Both the measured and calculated time delays appeared to be predicted by the time delay of the single scattering even when the single scattering was determined to be only a small portion of the time dependent response. The cumulative time distributions shown in Figures 1 through 5 are examples of the time distributions computed for some of the source and receiver configurations. The vertical dashed line in each of these plots indicate the center of a very short time interval during which the single scattered radiation arrives at the receiver. When both the source beam and the receiver are scanned off the source-receiver axis only that radiation which is single scattered in the volume formed by the intersection of the beam and the receiver field of view is detected. Since the intersection volume is so small, the single scattered response will arrive at the receiver in a very short time period centered about the time represented by the vertical dashed lines.

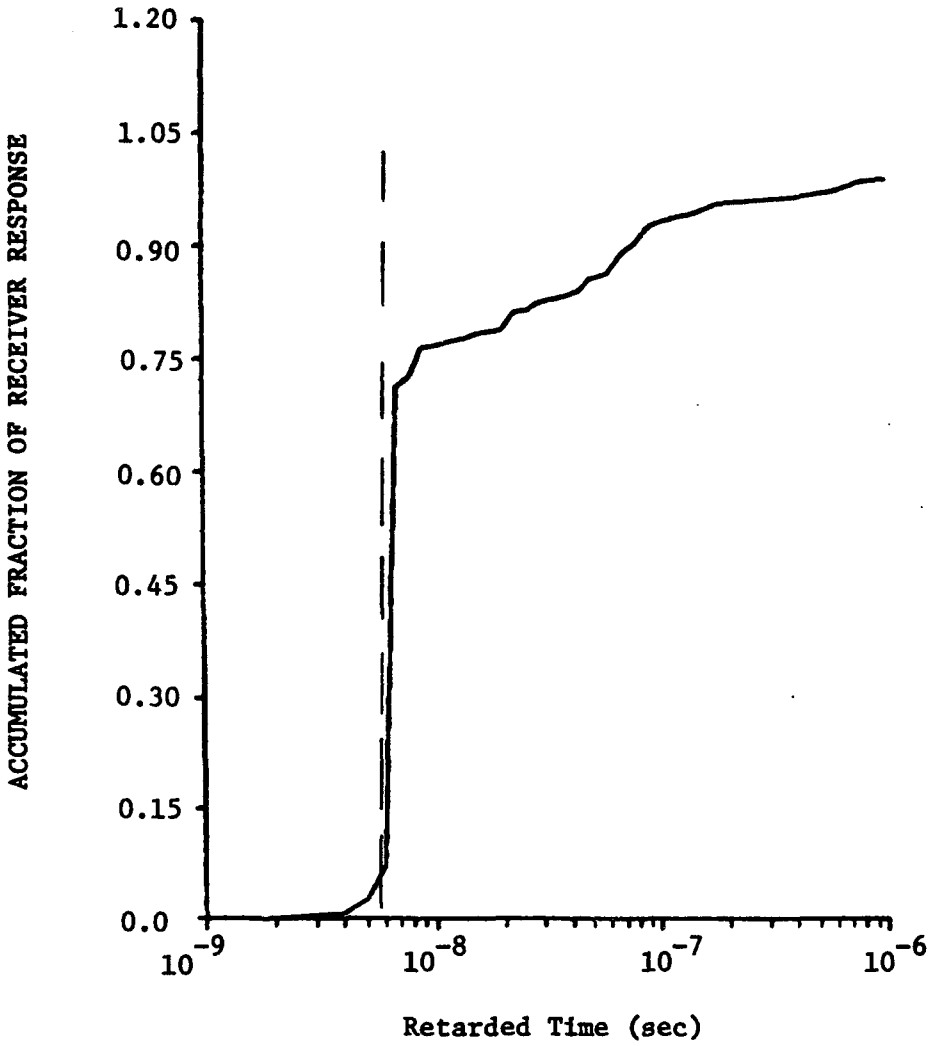

Fig. 1. Fractional Receiver Response Versus Retarded Time For 5^{o} Source Elevation and 3^{o} Receiver Elevation

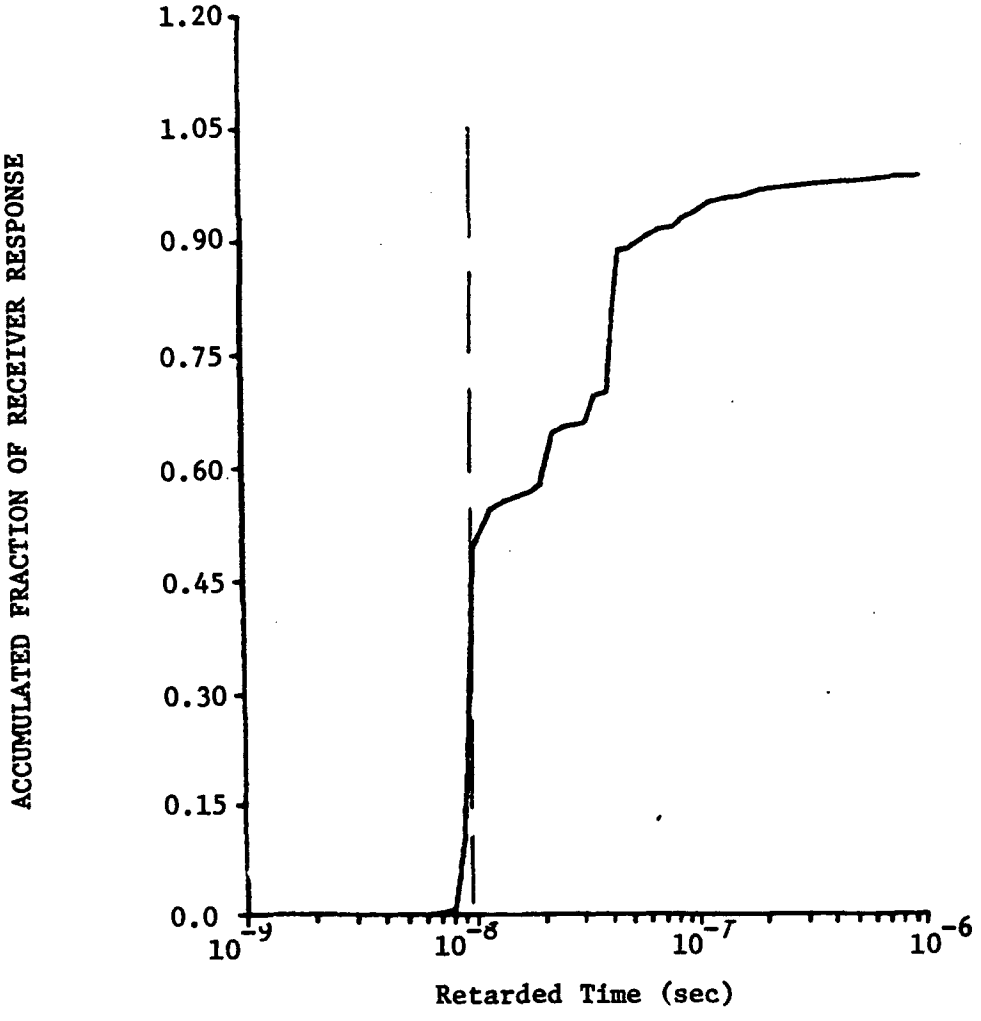

Fig. 2. Fractional Receiver Response Versus Retarded Time For 5° Source Elevation and 5° Receiver Elevation

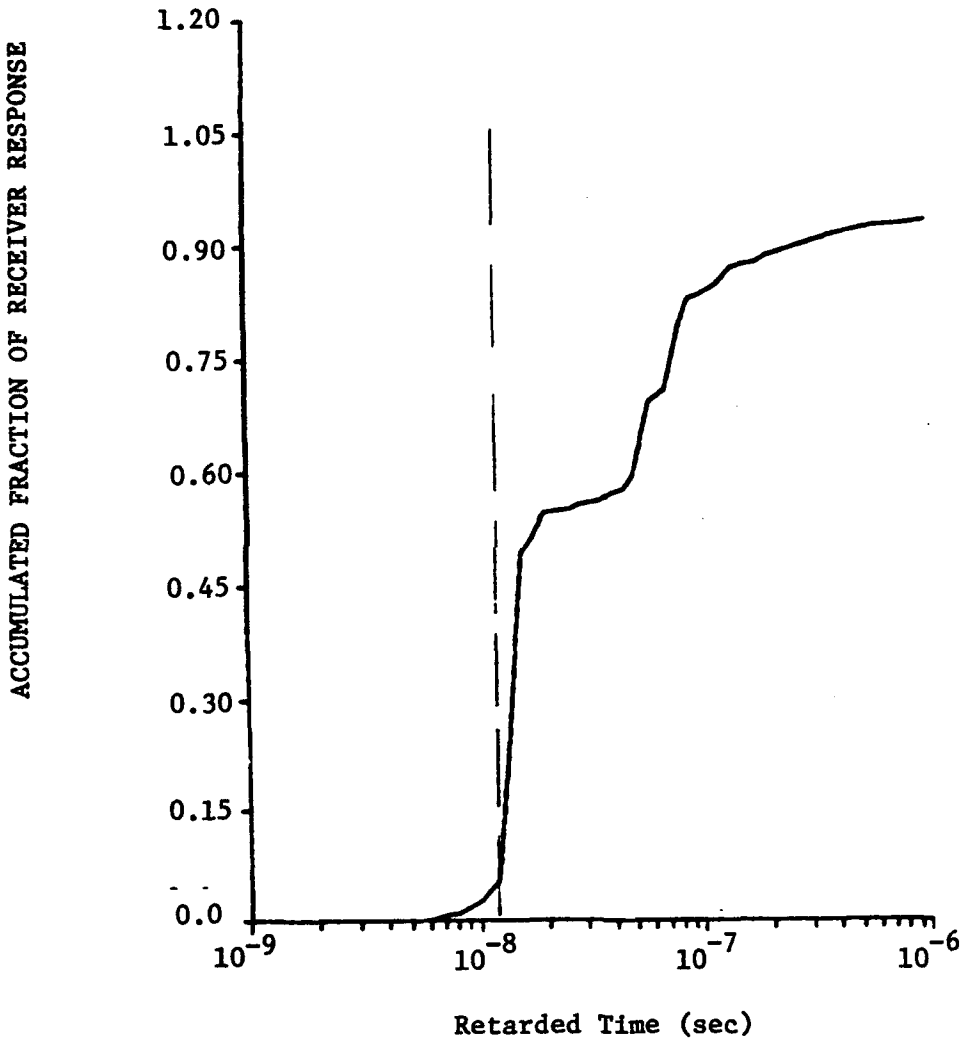

Fig. 3. Fractional Receiver Response Versus Retarded Time For 10° Source Elevation and 3° Receiver Elevation

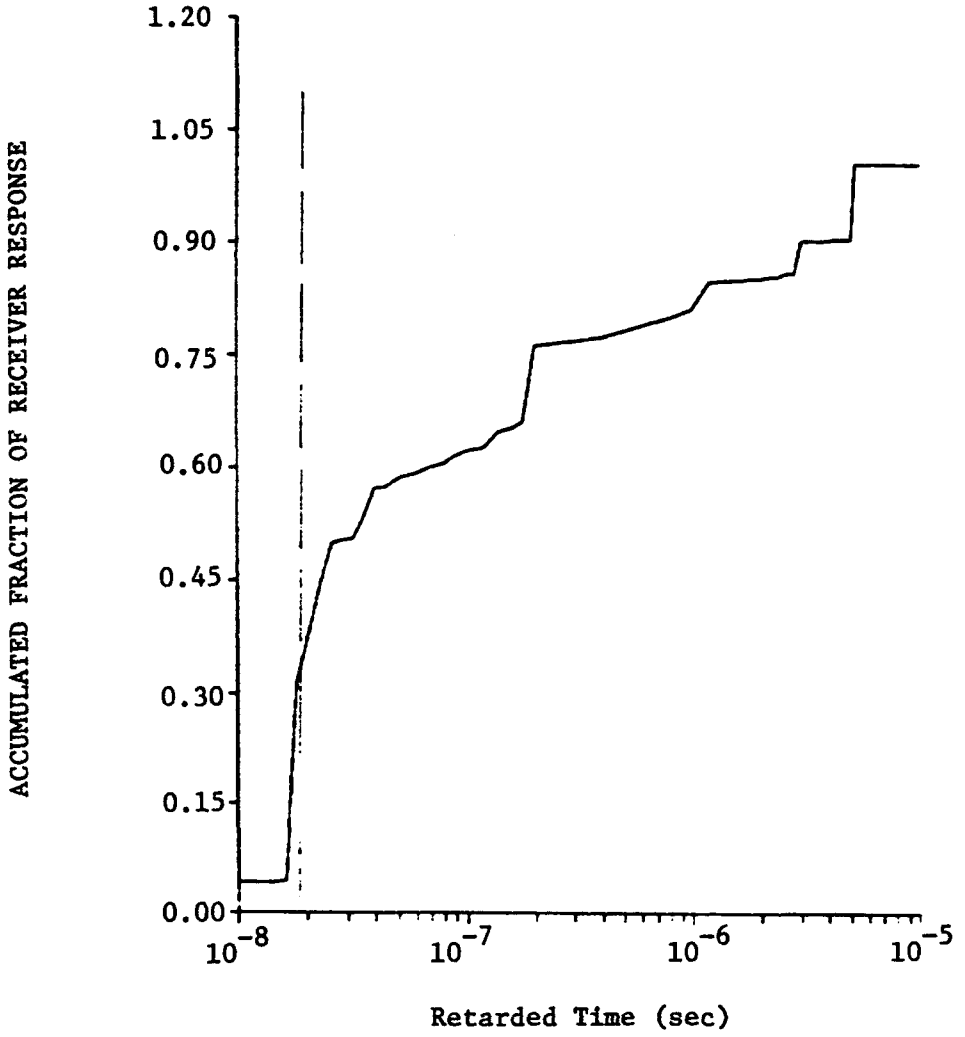

Fig. 4. Fractional Receiver Response Versus Retarded Time For 10° Source Elevation and 5° Receiver Elevation

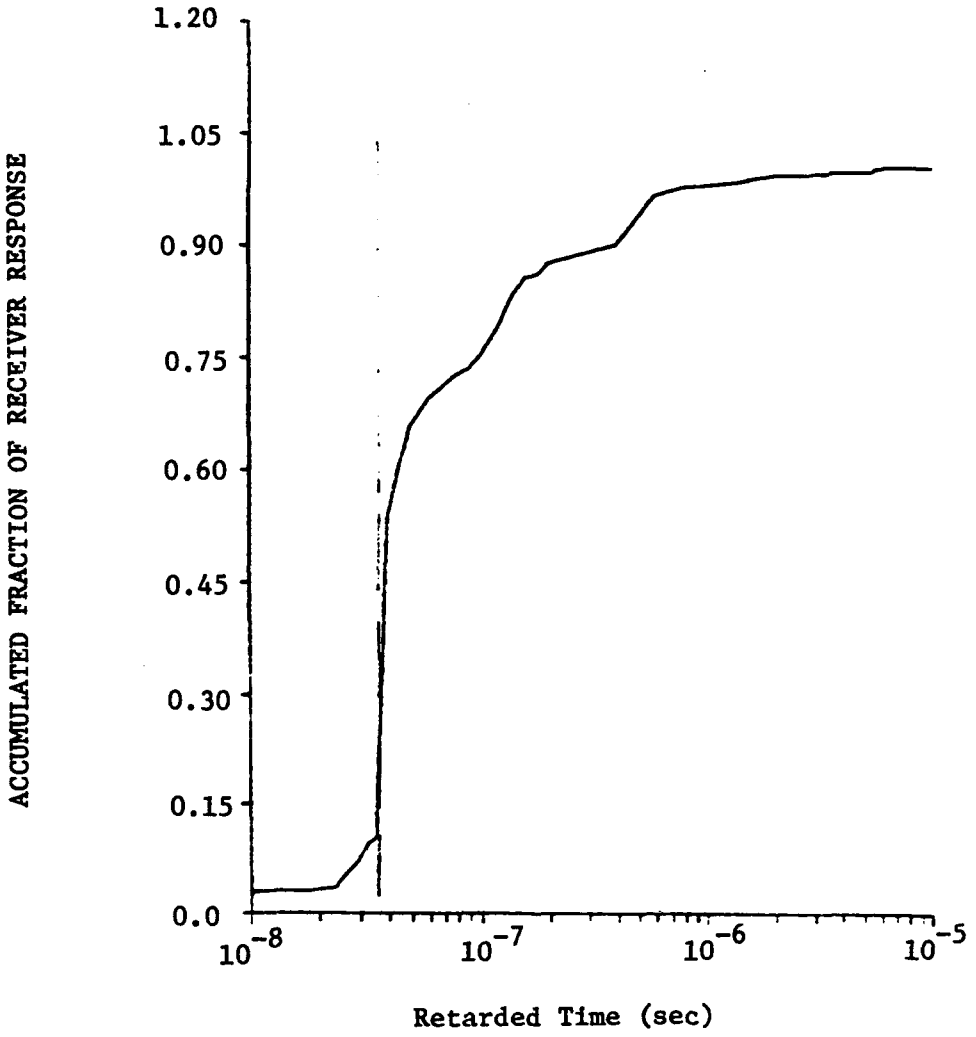

Fig. 5. Fractional Receiver Response Versus Retarded Time For 10^{o} Source Elevation and 10^{o} Receiver Elevation

Figures 1 through 5 show that the accumulative time response tends to rise sharply at approximately the time of the single scattered response. However, it should be noted that even in these examples approximately 50% or more of the responses are received after the time of the single scattered response and is spread over time periods of up to a microsecond or more.

Additional calculations were made for the source beam and receiver axis scanned as far as 30 degrees from the source-receiver axis. The cumulative time distributions for different orientations of the receiver axis for the source beam scanned at 15, 20 and 30 degrees off axis are shown in Figures 6, 7, and 8. Note that for the source scanned 15 degrees off the source-receiver axis the cumulative time distributions are very similiar for all the receiver directions except for the receiver scanned 5 degrees off axis. In that case the sharp rise in the distribution is near the single scattering time of arrival which is 29.48 nanoseconds. The expected retarded time of arrival of the single scattered response can be computed with the formula

$$T = D\ (((\sin\alpha + \sin\beta)/\sin(\alpha+\beta))-1.0)/V$$

where D is the source-receiver separation distance, V is the velocity of light, and α and β are the angles that the source beam and the axis of the receiver field of view are scanned off the source-receiver axis.

The cumulative time distributions for the source scanned 20 degrees off axis are quite dissimilar for the different receiver orientations. Since the differences in the cumulative time responses for the source beam rotated 15 and 30 degrees off the source-receiver axis are much less than those for 20° it is anticipated that the differences seem for the 20 degree source orientation is an anormaly caused by insufficient sampling in the TPART-III Monte Carlo program used for the calculation. The cumulative time distributions for the source beam rotated 30 degrees from the source receiver

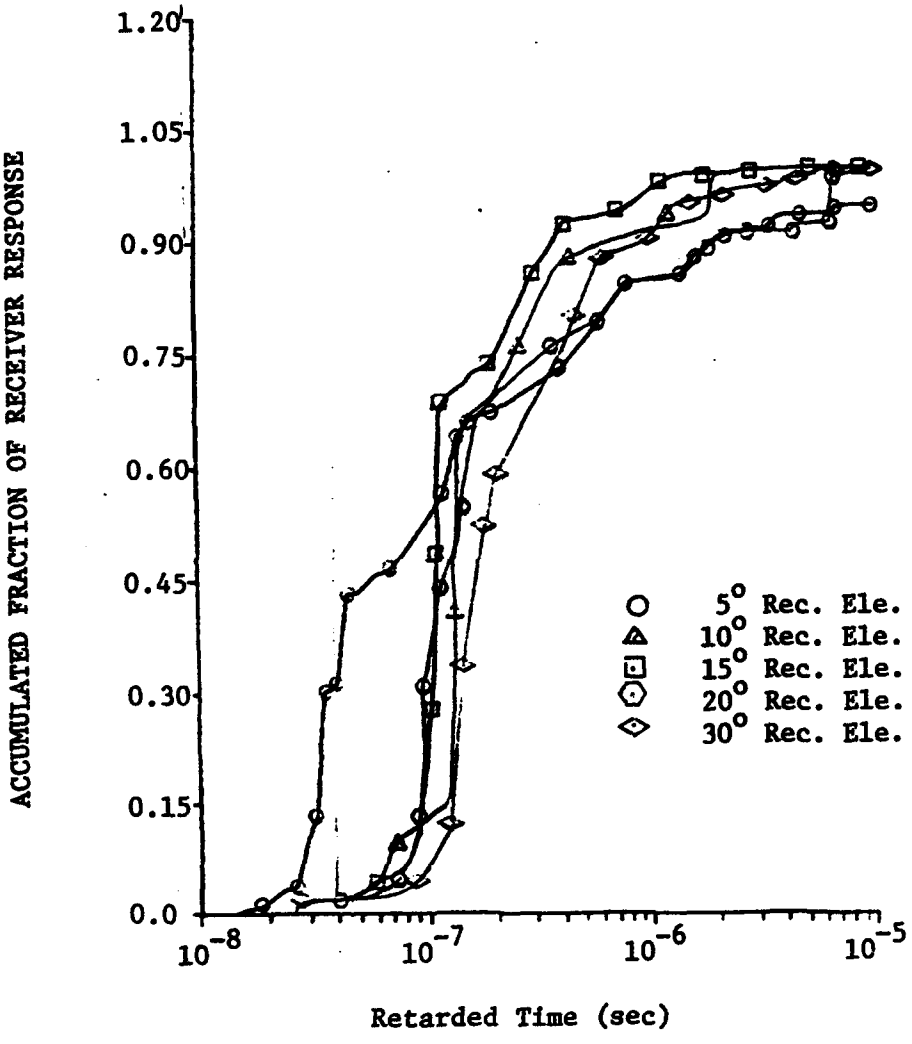

Fig. 6. Fractional Receiver Response Versus Retarded Time and Receiver Elevation For a 15° Source Elevation

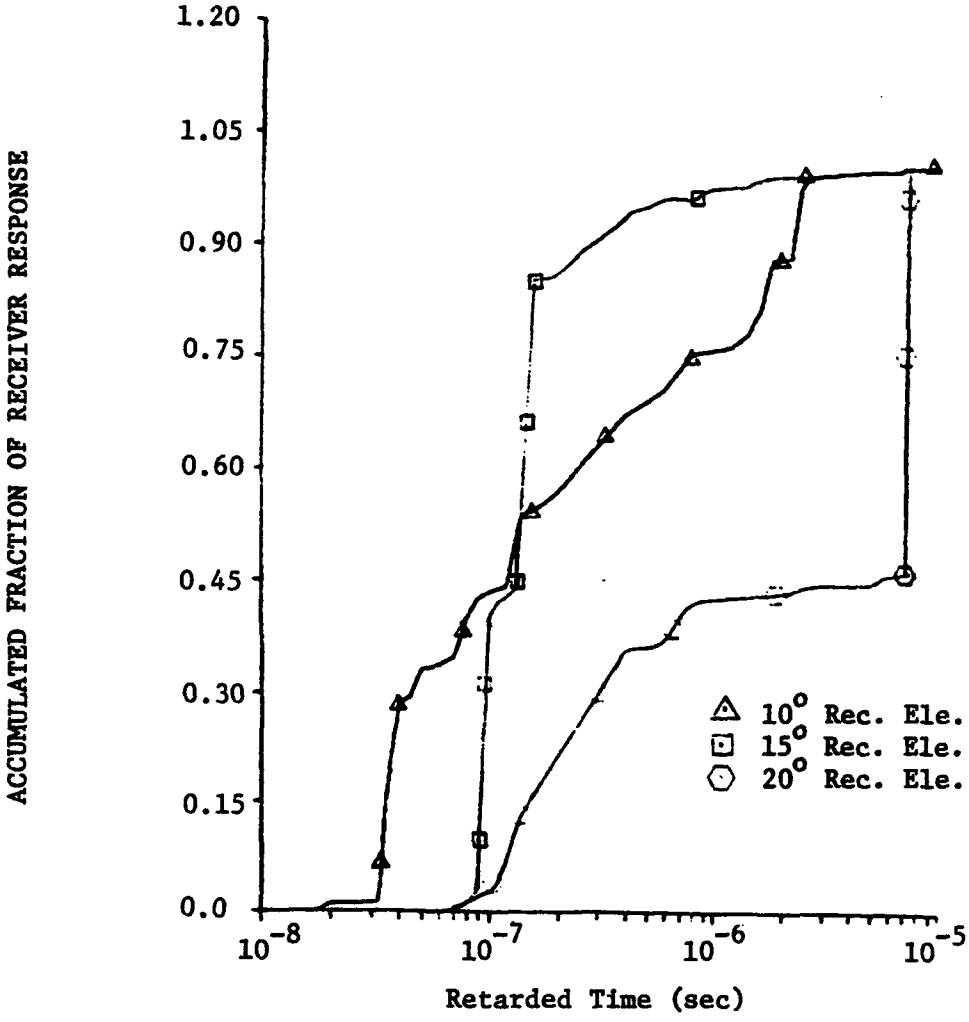

Fig. 7. Fractional Receiver Response Versus Retarded Time and Receiver Elevation For a 20^{o} Source Elevation

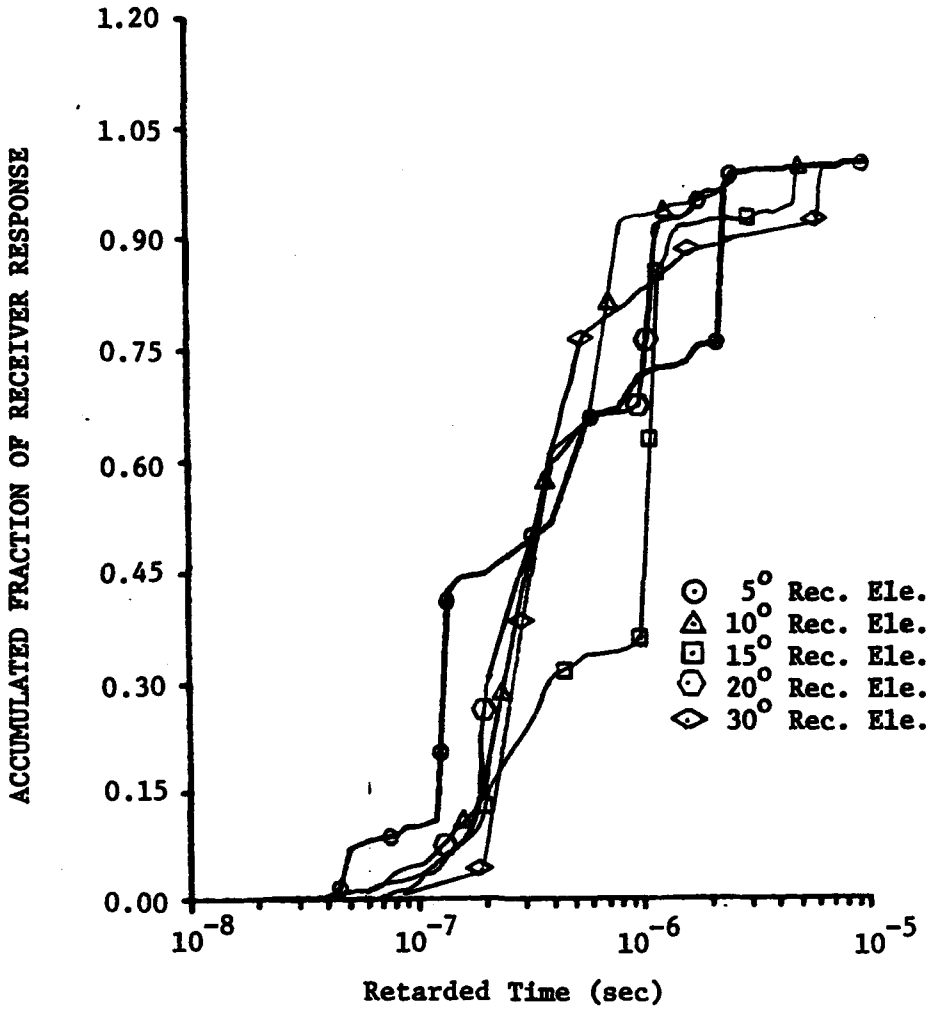

Fig. 8. Fractional Receiver Response Versus Retarded Time and Receiver Elevation For a 30° Source Elevation

for the 20 degree source orientation. If the whole group of curves for the 30 degree source orientation are compared with the set for the 15 degree source orientation, it is seen that in general the times of arrival are shifted to later times as the source beam is rotated farther from the source-receiver axis. It appears that the retarded time of arrival of the observed light intensity from the source rotated 30 degrees off axis is in the neighborhood of 1 microsecond.

Due to the cost of running the TPART-III program to generate time dependant transmission data for a large enough set of receiver directions and source directions to define the time distribution of the intensity received from 4π space for an isotropic source, a decision was made to supplement the TPART-III data with data calculated with the THART-L program. The THART-L program is designed to calculate the time dependent light intensity within each of a set of solid angle intervals defined about a receiver position due to point monodirectional source located at a given distance from the receiver within an infinite media. The direction of the source with respect to the source-receiver axis may be any angle from 0° to 180°. Thus one run of the THART-L program provides time dependent transmission data incident to the receiver from all directions rather than from one small solid angle interval as does the TPART-III program.

Table I lists the THART-L time and angular dependent results computed for a monodirectional source rotated 30 degrees from the source-receiver axis and located 765 meters from the receiver where both the source and receiver are assumed to be within an infinite cloud medium. Each entry listed in Table I is the fraction of the photons emitted which arrives per square meter at the receiver within the solid angle interval designated at the top of the column and in the time interval designated at the left of the column. The numbers in the bottom row are the numbers of photons within the solid angle intervals integrated over time.

TABLE I. TIME AND ANGULAR DISTRIBUTION OF THE SCATTERED INTENSITY 765 METERS FROM A MONODIRECTIONAL SOURCE SCANNED 30° OFF-AXIS IN AN INFINITE CLOUD MEDIUM. OPTICAL SEPARATION DISTANCE = 14.7

POLAR ANGLE		0.	0.	0.	0.	0.
		1.000E+01	1.000E+01	1.000E+01	1.000E+01	1.000E+01
AZIMUTHAL ANGLE		0.	1.125E+01	2.250E+01	4.500E+01	9.000E+01
		1.125E+01	2.250E+01	4.500E+01	9.000E+01	1.350E+02
TIME INTERVAL						
**********	-1.000E-07	9.582E-11	2.785E-11	1.835E-10	1.352E-10	3.896E-11
1.000E-07	-1.500E-07	4.632E-12	2.012E-12	3.705E-11	2.388E-10	2.937E-10
1.500E-07	-2.000E-07	2.908E-11	3.000E-12	2.682E-10	2.745E-11	2.542E-10
2.000E-07	-2.500E-07	1.302E-11	3.180E-10	2.354E-10	7.041E-11	1.612E-11
2.500E-07	-3.000E-07	1.002E-12	1.395E-12	2.308E-11	3.478E-11	6.392E-11
3.000E-07	-4.000E-07	6.756E-13	2.026E-14	7.478E-12	1.814E-10	9.599E-11
4.000E-07	-5.000E-07	3.109E-13	7.114E-14	4.526E-12	1.279E-11	1.501E-10
5.000E-07	-6.000E-07	1.018E-14	2.487E-15	9.447E-11	4.828E-14	6.137E-12
6.000E-07	-8.000E-07	1.572E-12	1.581E-14	2.746E-11	9.839E-11	7.109E-11
8.000E-07	-1.000E-06	1.098E-13	1.432E-14	3.142E-14	2.654E-12	2.928E-12
1.000E-06	-1.500E-06	5.025E-13	2.527E-12	3.843E-12	1.065E-11	2.806E-11
1.500E-06	-2.000E-06	3.405E-13	2.230E-13	2.269E-13	1.340E-12	1.077E-12
2.000E-06	-2.500E-06	4.658E-12	5.086E-12	1.005E-12	3.712E-13	3.537E-13
2.500E-06	-3.000E-06	2.636E-15	2.563E-15	1.861E-14	7.208E-14	1.598E-13
3.000E-06	-4.000E-06	5.192E-13	6.844E-14	4.334E-14	3.530E-13	3.007E-12
4.000E-06	-5.000E-06	1.667E-14	8.322E-15	1.326E-13	1.311E-11	9.302E-12
5.000E-06	-6.000E-06	1.169E-15	7.720E-15	2.220E-11	1.226E-13	2.006E-13
6.000E-06	-8.000E-06	2.467E-14	1.930E-14	2.037E-13	1.713E-12	1.186E-12
8.000E-06	-1.000E-05	6.632E-14	1.090E-13	8.339E-12	5.558E-11	1.379E-13
1.000E-05	-1.500E-05	0.	7.176E-48	0.	3.047E-39	4.098E-36
1.500E-05	-2.000E-05	0.	0.	0.	0.	0.
2.000E-05	-2.500E-05	0.	0.	0.	0.	0.
2.500E-05	-3.000E-05	0.	0.	0.	0.	0.
3.000E-05	-4.000E-05	0.	0.	0.	0.	0.
4.000E-05	-5.000E-05	0.	0.	0.	0.	0.
5.000E-05	-6.000E-05	0.	0.	0.	0.	0.
6.000E-05	-8.000E-05	0.	0.	0.	0.	0.
8.000E-05	-1.000E-04	0.	0.	0.	0.	0.
1.000E-04	-1.500E-04	0.	0.	0.	0.	0.
1.500E-04	-2.000E-04	0.	0.	0.	0.	0.
2.000E-04	-2.500E-04	0.	0.	0.	0.	0.
2.500E-04	-3.000E-04	0.	0.	0.	0.	0.
3.000E-04	-4.000E-04	0.	0.	0.	0.	0.
4.000E-04	-5.000E-04	0.	0.	0.	0.	0.
5.000E-04	-6.000E-04	0.	0.	0.	0.	0.
6.000E-04	-8.000E-04	0.	0.	0.	0.	0.
8.000E-04	-1.000E-03	0.	0.	0.	0.	0.
TOTAL		1.524E-10	3.604E-10	9.233E-10	9.368E-10	1.037E-09

****

TABLE I. (CONTINUED)

POLAR ANGLE	0.	1.000E+01	1.000E+01	1.000E+01	1.000E+01
	1.000E+01	2.000E+01	2.000E+01	2.000E+01	2.000E+01
AZIMUTHAL ANGLE	1.350E+02	0.	1.125E+01	2.250E+01	4.500E+01
	1.800E+02	1.125E+01	2.250E+01	4.500E+01	9.000E+01
TIME INTERVAL					
********** -1.000E-07	1.360E-11	6.233E-11	1.096E-11	4.357E-11	2.288E-11
1.000E-07 -1.500E-07	5.087E-12	6.739E-11	4.290E-11	1.605E-10	8.009E-11
1.500E-07 -2.000E-07	5.945E-10	7.119E-11	7.879E-11	1.242E-10	1.487E-09
2.000E-07 -2.500E-07	2.976E-10	5.812E-11	5.163E-10	8.147E-11	1.318E-10
2.500E-07 -3.000E-07	1.078E-09	1.586E-10	4.771E-11	6.831E-11	1.758E-11
3.000E-07 -4.000E-07	3.820E-12	1.690E-11	8.446E-10	5.133E-11	1.822E-10
4.000E-07 -5.000E-07	6.595E-11	1.423E-12	9.741E-13	2.398E-12	3.926E-12
5.000E-07 -6.000E-07	6.155E-13	2.001E-11	3.580E-12	1.559E-12	1.099E-12
6.000E-07 -8.000E-07	8.153E-13	1.132E-11	8.439E-13	3.490E-11	1.178E-10
8.000E-07 -1.000E-06	4.350E-14	9.082E-14	1.279E-09	1.901E-12	2.861E-11
1.000E-06 -1.500E-06	2.880E-11	1.967E-12	1.820E-11	8.482E-11	1.166E-09
1.500E-06 -2.000E-06	1.882E-10	4.249E-13	2.673E-13	5.252E-12	5.974E-12
2.000E-06 -2.500E-06	6.407E-13	6.424E-14	1.860E-12	6.982E-12	6.395E-12
2.500E-06 -3.000E-06	1.448E-14	1.638E-13	1.270E-13	3.791E-10	9.089E-10
3.000E-06 -4.000E-06	2.995E-12	5.774E-13	8.886E-13	1.311E-12	9.436E-12
4.000E-06 -5.000E-06	6.739E-12	2.120E-13	4.553E-14	2.363E-14	2.058E-11
5.000E-06 -6.000E-06	1.287E-12	1.544E-11	1.391E-11	2.768E-14	3.581E-12
6.000E-06 -8.000E-06	4.015E-14	1.260E-13	9.411E-13	3.255E-11	1.775E-11
8.000E-06 -1.000E-05	2.710E-14	6.560E-13	5.407E-11	2.092E-12	4.861E-12
1.000E-05 -1.500E-05	3.311E-35	5.458E-39	0.	1.263E-35	1.730E-36
1.500E-05 -2.000E-05	0.	0.	0.	0.	0.
2.000E-05 -2.500E-05	0.	0.	0.	0.	0.
2.500E-05 -3.000E-05	0.	0.	0.	0.	0.
3.000E-05 -4.000E-05	0.	0.	0.	0.	0.
4.000E-05 -5.000E-05	0.	0.	0.	0.	0.
5.000E-05 -6.000E-05	0.	0.	0.	0.	0.
6.000E-05 -8.000E-05	0.	0.	0.	0.	0.
8.000E-05 -1.000E-04	0.	0.	0.	0.	0.
1.000E-04 -1.500E-04	0.	0.	0.	0.	0.
1.500E-04 -2.000E-04	0.	0.	0.	0.	0.
2.000E-04 -2.500E-04	0.	0.	0.	0.	0.
2.500E-04 -3.000E-04	0.	0.	0.	0.	0.
3.000E-04 -4.000E-04	0.	0.	0.	0.	0.
4.000E-04 -5.000E-04	0.	0.	0.	0.	0.
5.000E-04 -6.000E-04	0.	0.	0.	0.	0.
6.000E-04 -8.000E-04	0.	0.	0.	0.	0.
8.000E-04 -1.000E-03	0.	0.	0.	0.	0.
TOTAL	2.289E-09	4.970E-10	2.917E-09	1.082E-09	1.760E-08

****

TABLE I. (CONTINUED)

POLAR ANGLE		1.000E+01	1.000E+01	2.000E+01	2.000E+01	2.000E+01
		2.000E+01	2.000E+01	3.000E+01	3.000E+01	3.000E+01
AZIMUTHAL ANGLE		9.000E+01	1.350E+02	0.	1.125E+01	2.250E+01
		1.350E+02	1.800E+02	1.125E+01	2.250E+01	4.500E+01
TIME INTERVAL						
*********	-1.000E-07	2.123E-10	1.488E-08	0.	0.	1.504E-10
1.000E-07	-1.500E-07	5.011E-10	9.718E-12	1.727E-11	2.868E-10	5.334E-11
1.500E-07	-2.000E-07	7.528E-11	1.325E-09	1.638E-11	2.581E-11	4.781E-11
2.000E-07	-2.500E-07	6.451E-11	1.576E-11	2.886E-10	6.335E-11	5.970E-11
2.500E-07	-3.000E-07	1.589E-11	4.262E-11	1.677E-11	4.345E-11	5.649E-10
3.000E-07	-4.000E-07	5.649E-10	1.868E-10	1.894E-11	1.011E-10	1.270E-09
4.000E-07	-5.000E-07	2.130E-12	8.627E-11	1.875E-10	5.189E-11	3.569E-11
5.000E-07	-6.000E-07	2.291E-11	8.513E-13	3.471E-12	3.404E-12	3.945E-12
6.000E-07	-8.000E-07	1.451E-11	1.534E-10	7.825E-12	1.157E-11	2.482E-12
8.000E-07	-1.000E-06	1.119E-11	8.908E-11	1.415E-12	1.455E-11	4.154E-12
1.000E-06	-1.500E-06	5.936E-10	3.816E-12	8.044E-12	5.114E-11	3.844E-10
1.500E-06	-2.000E-06	8.284E-11	4.395E-12	6.048E-12	3.713E-12	9.798E-12
2.000E-06	-2.500E-06	4.092E-12	4.730E-13	3.328E-12	2.274E-13	1.281E-11
2.500E-06	-3.000E-06	1.950E-12	2.182E-12	2.361E-14	2.190E-13	1.026E-12
3.000E-06	-4.000E-06	4.096E-11	1.354E-11	2.227E-13	3.715E-12	7.420E-12
4.000E-06	-5.000E-06	4.049E-13	1.296E-13	1.495E-13	9.941E-14	2.295E-12
5.000E-06	-6.000E-06	9.406E-13	1.323E-11	1.400E-11	5.761E-13	9.503E-13
6.000E-06	-8.000E-06	2.598E-12	1.405E-12	8.216E-12	2.184E-11	3.836E-12
8.000E-06	-1.000E-05	1.542E-11	7.173E-13	1.047E-13	6.959E-12	3.825E-12
1.000E-05	-1.500E-05	1.739E-28	2.301E-32	1.984E-34	5.034E-33	6.922E-36
1.500E-05	-2.000E-05	0.	0.	0.	0.	0.
2.000E-05	-2.500E-05	0.	0.	0.	0.	0.
2.500E-05	-3.000E-05	0.	0.	0.	0.	0.
3.000E-05	-4.000E-05	0.	0.	0.	0.	0.
4.000E-05	-5.000E-05	0.	0.	0.	0.	0.
5.000E-05	-6.000E-05	0.	0.	0.	0.	0.
6.000E-05	-8.000E-05	0.	0.	0.	0.	0.
8.000E-05	-1.000E-04	0.	0.	0.	0.	0.
1.000E-04	-1.500E-04	0.	0.	0.	0.	0.
1.500E-04	-2.000E-04	0.	0.	0.	0.	0.
2.000E-04	-2.500E-04	0.	0.	0.	0.	0.
2.500E-04	-3.000E-04	0.	0.	0.	0.	0.
3.000E-04	-4.000E-04	0.	0.	0.	0.	0.
4.000E-04	-5.000E-04	0.	0.	0.	0.	0.
5.000E-04	-6.000E-04	0.	0.	0.	0.	0.
6.000E-04	-8.000E-04	0.	0.	0.	0.	0.
8.000E-04	-1.000E-03	0.	0.	0.	0.	0.
TOTAL		2.227E-09	1.683E-08	5.984E-10	6.903E-10	2.619E-09

****

TABLE I. (CONTINUED)

POLAR ANGLE		2.000E+01	2.000E+01	2.000E+01	3.000E+01	3.000E+01
		3.000E+01	3.000E+01	3.000E+01	4.500E+01	4.500E+01
AZIMUTHAL ANGLE		4.500E+01	9.000E+01	1.350E+02	0.	1.125E+01
		9.000E+01	1.350E+02	1.800E+02	1.125E+01	2.250E+01
TIME INTERVAL						
**********	-1.000E-07	2.519E-10	3.947E-10	0.	0.	0.
1.000E-07	-1.500E-07	3.186E-11	1.206E-11	2.051E-11	0.	0.
1.500E-07	-2.000E-07	9.749E-10	1.583E-11	9.680E-12	8.534E-11	1.276E-11
2.000E-07	-2.500E-07	2.574E-10	4.102E-10	1.937E-11	6.193E-10	1.567E-11
2.500E-07	-3.000E-07	9.873E-10	1.358E-11	8.111E-12	1.410E-10	2.220E-11
3.000E-07	-4.000E-07	1.253E-10	1.905E-10	1.477E-09	2.315E-10	5.511E-10
4.000E-07	-5.000E-07	1.051E-10	1.311E-11	2.635E-11	8.765E-11	1.400E-09
5.000E-07	-6.000E-07	4.409E-11	3.721E-10	4.494E-12	9.089E-11	1.222E-10
6.000E-07	-8.000E-07	1.823E-10	1.093E-11	2.309E-12	9.733E-12	5.476E-11
8.000E-07	-1.000E-06	2.960E-08	7.445E-12	2.570E-12	7.905E-12	1.904E-11
1.000E-06	-1.500E-06	1.081E-10	2.755E-09	5.828E-12	6.920E-11	1.632E-10
1.500E-06	-2.000E-06	4.369E-11	1.241E-10	1.173E-11	7.341E-13	1.105E-11
2.000E-06	-2.500E-06	2.776E-11	3.021E-11	2.031E-11	8.210E-12	3.607E-11
2.500E-06	-3.000E-06	2.109E-12	3.061E-09	1.797E-11	1.805E-12	4.013E-12
3.000E-06	-4.000E-06	1.274E-10	2.407E-11	4.337E-11	5.916E-12	2.327E-12
4.000E-06	-5.000E-06	6.905E-12	1.323E-11	2.431E-11	4.199E-13	4.521E-14
5.000E-06	-6.000E-06	9.442E-13	3.522E-12	1.723E-11	4.828E-12	1.661E-12
6.000E-06	-8.000E-06	3.121E-12	3.457E-11	7.734E-11	3.932E-10	1.110E-11
8.000E-06	-1.000E-05	5.768E-11	3.602E-12	8.022E-13	1.184E-11	2.666E-10
1.000E-05	-1.500E-05	3.844E-23	1.259E-34	8.435E-35	7.673E-31	7.600E-33
1.500E-05	-2.000E-05	0.	0.	0.	0.	0.
2.000E-05	-2.500E-05	0.	0.	0.	0.	0.
2.500E-05	-3.000E-05	0.	0.	0.	0.	0.
3.000E-05	-4.000E-05	0.	0.	0.	0.	0.
4.000E-05	-5.000E-05	0.	0.	0.	0.	0.
5.000E-05	-6.000E-05	0.	0.	0.	0.	0.
6.000E-05	-8.000E-05	0.	0.	0.	0.	0.
8.000E-05	-1.000E-04	0.	0.	0.	0.	0.
1.000E-04	-1.500E-04	0.	0.	0.	0.	0.
1.500E-04	-2.000E-04	0.	0.	0.	0.	0.
2.000E-04	-2.500E-04	0.	0.	0.	0.	0.
2.500E-04	-3.000E-04	0.	0.	0.	0.	0.
3.000E-04	-4.000E-04	0.	0.	0.	0.	0.
4.000E-04	-5.000E-04	0.	0.	0.	0.	0.
5.000E-04	-6.000E-04	0.	0.	0.	0.	0.
6.000E-04	-8.000E-04	0.	0.	0.	0.	0.
8.000E-04	-1.000E-03	0.	0.	0.	0.	0.
TOTAL		3.293E-08	7.489E-09	1.791E-09	1.770E-09	2.694E-09

****

TABLE I. (CONTINUED)

POLAR ANGLE		3.000E+01	3.000E+01	3.000E+01	3.000E+01	4.500E+01
		4.500E+01	4.500E+01	4.500E+01	4.500E+01	6.000E+01
AZIMUTHAL ANGLE		2.250E+01	4.500E+01	9.000E+01	1.350E+02	0.
		4.500E+01	9.000E+01	1.350E+02	1.800E+02	1.125E+01
TIME INTERVAL						
*********	-1.000E-07	0.	0.	1.169E-09	0.	0.
1.000E-07	-1.500E-07	0.	2.247E-10	3.245E-11	0.	0.
1.500E-07	-2.000E-07	9.511E-12	1.855E-11	4.787E-10	2.492E-10	0.
2.000E-07	-2.500E-07	1.275E-10	1.493E-09	4.404E-10	6.063E-10	1.513E-09
2.500E-07	-3.000E-07	1.448E-10	4.964E-10	9.108E-10	4.777E-12	1.235E-10
3.000E-07	-4.000E-07	3.964E-10	9.862E-10	9.506E-10	1.429E-10	1.332E-10
4.000E-07	-5.000E-07	1.910E-10	1.345E-10	1.554E-10	3.751E-10	9.206E-11
5.000E-07	-6.000E-07	6.709E-11	1.171E-09	3.986E-11	1.550E-11	3.972E-08
6.000E-07	-8.000E-07	1.059E-10	6.767E-10	5.521E-10	2.020E-10	5.902E-11
8.000E-07	-1.000E-06	9.834E-12	1.102E-10	4.236E-11	4.128E-11	2.227E-11
1.000E-06	-1.500E-06	9.854E-10	1.984E-10	1.077E-10	3.849E-10	1.092E-11
1.500E-06	-2.000E-06	4.603E-11	2.473E-09	1.131E-10	7.459E-11	2.570E-12
2.000E-06	-2.500E-06	5.438E-12	7.494E-11	6.552E-12	9.955E-11	6.452E-12
2.500E-06	-3.000E-06	5.214E-12	2.992E-11	2.379E-10	1.217E-11	1.883E-12
3.000E-06	-4.000E-06	3.634E-12	1.485E-10	7.196E-11	1.678E-11	1.677E-12
4.000E-06	-5.000E-06	3.334E-12	2.095E-10	3.625E-11	1.013E-10	1.808E-12
5.000E-06	-6.000E-06	1.655E-12	1.414E-12	1.303E-10	2.027E-10	9.290E-13
6.000E-06	-8.000E-06	6.272E-10	7.720E-12	6.003E-10	5.909E-12	3.516E-12
8.000E-06	-1.000E-05	1.133E-12	1.857E-10	8.547E-11	4.477E-10	3.218E-13
1.000E-05	-1.500E-05	4.122E-31	2.652E-30	3.377E-31	7.998E-31	4.646E-29
1.500E-05	-2.000E-05	0.	0.	0.	0.	0.
2.000E-05	-2.500E-05	0.	0.	0.	0.	0.
2.500E-05	-3.000E-05	0.	0.	0.	0.	0.
3.000E-05	-4.000E-05	0.	0.	0.	0.	0.
4.000E-05	-5.000E-05	0.	0.	0.	0.	0.
5.000E-05	-6.000E-05	0.	0.	0.	0.	0.
6.000E-05	-8.000E-05	0.	0.	0.	0.	0.
8.000E-05	-1.000E-04	0.	0.	0.	0.	0.
1.000E-04	-1.500E-04	0.	0.	0.	0.	0.
1.500E-04	-2.000E-04	0.	0.	0.	0.	0.
2.000E-04	-2.500E-04	0.	0.	0.	0.	0.
2.500E-04	-3.000E-04	0.	0.	0.	0.	0.
3.000E-04	-4.000E-04	0.	0.	0.	0.	0.
4.000E-04	-5.000E-04	0.	0.	0.	0.	0.
5.000E-04	-6.000E-04	0.	0.	0.	0.	0.
6.000E-04	-8.000E-04	0.	0.	0.	0.	0.
8.000E-04	-1.000E-03	0.	0.	0.	0.	0.
TOTAL		2.731E-09	8.641E-09	6.161E-09	2.983E-09	4.181E-08

****

TABLE I. (CONTINUED)

POLAR ANGLE		4.500E+01	4.500E+01	4.500E+01	4.500E+01	4.500E+01
		6.000E+01	6.000E+01	6.000E+01	6.000E+01	6.000E+01
AZIMUTHAL ANGLE		1.125E+01	2.250E+01	4.500E+01	9.000E+01	1.350E+02
		2.250E+01	4.500E+01	9.000E+01	1.350E+02	1.800E+02
TIME INTERVAL						
*********	-1.000E-07	0.	0.	0.	0.	0.
1.000E-07	-1.500E-07	0.	0.	0.	0.	0.
1.500E-07	-2.000E-07	0.	0.	3.229E-10	1.143E-10	0.
2.000E-07	-2.500E-07	6.390E-11	0.	2.972E-10	4.772E-11	0.
2.500E-07	-3.000E-07	9.897E-12	1.988E-12	0.	8.219E-10	2.446E-10
3.000E-07	-4.000E-07	1.058E-11	9.579E-11	1.660E-09	9.678E-11	2.422E-10
4.000E-07	-5.000E-07	3.450E-11	1.463E-10	1.374E-10	1.914E-10	4.204E-11
5.000E-07	-6.000E-07	9.170E-11	7.103E-10	4.669E-11	1.803E-10	4.025E-11
6.000E-07	-8.000E-07	8.653E-11	3.293E-10	6.206E-10	5.514E-11	2.478E-11
8.000E-07	-1.000E-06	3.341E-11	7.050E-11	3.191E-10	3.152E-11	1.640E-11
1.000E-06	-1.500E-06	2.012E-11	1.026E-09	8.780E-10	1.130E-10	4.635E-09
1.500E-06	-2.000E-06	2.212E-11	1.144E-10	7.389E-11	6.454E-11	2.632E-11
2.000E-06	-2.500E-06	4.647E-11	1.229E-11	9.132E-11	1.507E-11	9.352E-11
2.500E-06	-3.000E-06	5.451E-12	1.002E-10	4.275E-11	2.582E-11	4.434E-10
3.000E-06	-4.000E-06	3.368E-12	3.334E-10	2.873E-09	3.168E-10	5.103E-11
4.000E-06	-5.000E-06	9.189E-13	1.401E-10	4.463E-12	6.879E-11	4.591E-10
5.000E-06	-6.000E-06	3.462E-11	6.779E-11	6.273E-12	2.588E-10	3.190E-09
6.000E-06	-8.000E-06	1.030E-11	2.242E-10	3.414E-11	6.364E-11	2.922E-10
8.000E-06	-1.000E-05	3.186E-11	3.296E-10	2.529E-11	8.040E-11	2.384E-10
1.000E-05	-1.500E-05	3.013E-34	1.609E-31	1.230E-26	7.096E-30	7.028E-31
1.500E-05	-2.000E-05	0.	0.	0.	0.	0.
2.000E-05	-2.500E-05	0.	0.	0.	0.	0.
2.500E-05	-3.000E-05	0.	0.	0.	0.	0.
3.000E-05	-4.000E-05	0.	0.	0.	0.	0.
4.000E-05	-5.000E-05	0.	0.	0.	0.	0.
5.000E-05	-6.000E-05	0.	0.	0.	0.	0.
6.000E-05	-8.000E-05	0.	0.	0.	0.	0.
8.000E-05	-1.000E-04	0.	0.	0.	0.	0.
1.000E-04	-1.500E-04	0.	0.	0.	0.	0.
1.500E-04	-2.000E-04	0.	0.	0.	0.	0.
2.000E-04	-2.500E-04	0.	0.	0.	0.	0.
2.500E-04	-3.000E-04	0.	0.	0.	0.	0.
3.000E-04	-4.000E-04	0.	0.	0.	0.	0.
4.000E-04	-5.000E-04	0.	0.	0.	0.	0.
5.000E-04	-6.000E-04	0.	0.	0.	0.	0.
6.000E-04	-8.000E-04	0.	0.	0.	0.	0.
8.000E-04	-1.000E-03	0.	0.	0.	0.	0.
TOTAL		5.057E-10	3.702E-09	7.633E-09	2.525E-09	1.004E-08

****

TABLE I. (CONTINUED)

POLAR ANGLE		6.000E+01	6.000E+01	6.000E+01	6.000E+01	6.000E+01
		7.500E+01	7.500E+01	7.500E+01	7.500E+01	7.500E+01
AZIMUTHAL ANGLE		0.	1.125E+01	2.250E+01	4.500E+01	9.000E+01
		1.125E+01	2.250E+01	4.500E+01	9.000E+01	1.350E+02
TIME INTERVAL						
*********	-1.000E-07	0.	0.	0.	0.	0.
1.000E-07	-1.500E-07	0.	0.	0.	0.	0.
1.500E-07	-2.000E-07	0.	0.	0.	0.	0.
2.000E-07	-2.500E-07	0.	0.	0.	0.	5.206E-11
2.500E-07	-3.000E-07	0.	2.305E-11	6.985E-12	9.594E-12	1.657E-10
3.000E-07	-4.000E-07	1.229E-11	1.721E-11	1.644E-12	1.100E-09	1.130E-11
4.000E-07	-5.000E-07	7.383E-12	1.754E-11	1.301E-10	3.810E-11	7.458E-11
5.000E-07	-6.000E-07	1.294E-10	1.204E-11	3.038E-10	1.127E-11	1.225E-09
6.000E-07	-8.000E-07	4.174E-10	5.691E-11	1.281E-10	1.549E-10	5.025E-11
8.000E-07	-1.000E-06	5.717E-10	6.464E-12	5.570E-11	7.730E-11	4.320E-11
1.000E-06	-1.500E-06	3.257E-11	5.829E-12	7.867E-10	2.018E-10	4.048E-10
1.500E-06	-2.000E-06	2.775E-11	2.009E-11	6.684E-11	5.334E-11	1.964E-10
2.000E-06	-2.500E-06	3.592E-11	8.436E-11	7.103E-11	9.012E-11	1.641E-10
2.500E-06	-3.000E-06	7.505E-12	7.173E-13	1.250E-11	1.479E-10	5.671E-11
3.000E-06	-4.000E-06	4.688E-12	2.502E-10	1.651E-11	6.461E-11	1.746E-10
4.000E-06	-5.000E-06	2.850E-12	2.769E-12	3.600E-10	1.131E-10	6.298E-12
5.000E-06	-6.000E-06	2.403E-12	1.932E-10	1.383E-11	2.459E-11	6.144E-11
6.000E-06	-8.000E-06	5.339E-11	1.298E-10	3.349E-11	1.871E-10	3.957E-11
8.000E-06	-1.000E-05	1.695E-11	2.855E-11	7.272E-12	3.487E-11	2.373E-10
1.000E-05	-1.500E-05	3.845E-30	4.847E-27	2.273E-30	1.920E-25	2.399E-23
1.500E-05	-2.000E-05	0.	0.	0.	0.	0.
2.000E-05	-2.500E-05	0.	0.	0.	0.	0.
2.500E-05	-3.000E-05	0.	0.	0.	0.	0.
3.000E-05	-4.000E-05	0.	0.	0.	0.	0.
4.000E-05	-5.000E-05	0.	0.	0.	0.	0.
5.000E-05	-6.000E-05	0.	0.	0.	0.	0.
6.000E-05	-8.000E-05	0.	0.	0.	0.	0.
8.000E-05	-1.000E-04	0.	0.	0.	0.	0.
1.000E-04	-1.500E-04	0.	0.	0.	0.	0.
1.500E-04	-2.000E-04	0.	0.	0.	0.	0.
2.000E-04	-2.500E-04	0.	0.	0.	0.	0.
2.500E-04	-3.000E-04	0.	0.	0.	0.	0.
3.000E-04	-4.000E-04	0.	0.	0.	0.	0.
4.000E-04	-5.000E-04	0.	0.	0.	0.	0.
5.000E-04	-6.000E-04	0.	0.	0.	0.	0.
6.000E-04	-8.000E-04	0.	0.	0.	0.	0.
8.000E-04	-1.000E-03	0.	0.	0.	0.	0.
TOTAL		1.383E-09	8.597E-10	2.054E-09	2.309E-09	2.953E-09

****

TABLE I. (CONTINUED)

POLAR ANGLE		6.000E+01	7.500E+01	7.500E+01	7.500E+01	7.500E+01
		7.500E+01	9.000E+01	9.000E+01	9.000E+01	9.000E+01
AZIMUTHAL ANGLE		1.350E+02	0.	1.125E+01	2.250E+01	4.500E+01
		1.800E+02	1.125E+01	2.250E+01	4.500E+01	9.000E+01
TIME INTERVAL						
*********	-1.000E-07	0.	0.	0.	0.	0.
1.000E-07	-1.500E-07	0.	0.	0.	0.	0.
1.500E-07	-2.000E-07	0.	0.	0.	0.	0.
2.000E-07	-2.500E-07	0.	0.	0.	6.175E-12	0.
2.500E-07	-3.000E-07	0.	0.	0.	0.	0.
3.000E-07	-4.000E-07	1.165E-10	7.072E-11	0.	0.	9.391E-12
4.000E-07	-5.000E-07	1.830E-11	9.036E-11	2.129E-09	7.317E-12	0.
5.000E-07	-6.000E-07	1.118E-11	1.227E-11	9.042E-12	1.136E-09	1.065E-11
6.000E-07	-8.000E-07	8.269E-11	2.860E-10	3.165E-11	8.206E-11	9.353E-11
8.000E-07	-1.000E-06	7.894E-12	7.986E-12	1.255E-11	3.432E-11	3.679E-11
1.000E-06	-1.500E-06	3.814E-11	2.794E-11	4.267E-11	1.770E-11	6.358E-11
1.500E-06	-2.000E-06	9.669E-11	1.181E-10	1.544E-11	1.337E-11	4.077E-10
2.000E-06	-2.500E-06	1.877E-11	9.419E-11	5.562E-11	1.198E-10	2.548E-10
2.500E-06	-3.000E-06	2.051E-10	1.290E-12	1.472E-12	2.066E-12	1.654E-10
3.000E-06	-4.000E-06	9.157E-10	6.554E-12	5.585E-12	9.798E-11	5.361E-10
4.000E-06	-5.000E-06	1.260E-10	7.985E-12	5.283E-12	4.440E-11	1.076E-10
5.000E-06	-6.000E-06	3.922E-11	1.512E-12	1.784E-11	3.948E-12	4.442E-11
6.000E-06	-8.000E-06	4.237E-10	3.333E-09	4.103E-12	3.268E-11	8.914E-11
8.000E-06	-1.000E-05	3.114E-10	3.015E-09	7.559E-11	7.197E-12	6.353E-11
1.000E-05	-1.500E-05	4.266E-29	2.679E-25	9.933E-30	5.057E-29	4.126E-30
1.500E-05	-2.000E-05	0.	0.	0.	0.	0.
2.000E-05	-2.500E-05	0.	0.	0.	0.	0.
2.500E-05	-3.000E-05	0.	0.	0.	0.	0.
3.000E-05	-4.000E-05	0.	0.	0.	0.	0.
4.000E-05	-5.000E-05	0.	0.	0.	0.	0.
5.000E-05	-6.000E-05	0.	0.	0.	0.	0.
6.000E-05	-8.000E-05	0.	0.	0.	0.	0.
8.000E-05	-1.000E-04	0.	0.	0.	0.	0.
1.000E-04	-1.500E-04	0.	0.	0.	0.	0.
1.500E-04	-2.000E-04	0.	0.	0.	0.	0.
2.000E-04	-2.500E-04	0.	0.	0.	0.	0.
2.500E-04	-3.000E-04	0.	0.	0.	0.	0.
3.000E-04	-4.000E-04	0.	0.	0.	0.	0.
4.000E-04	-5.000E-04	0.	0.	0.	0.	0.
5.000E-04	-6.000E-04	0.	0.	0.	0.	0.
6.000E-04	-8.000E-04	0.	0.	0.	0.	0.
8.000E-04	-1.000E-03	0.	0.	0.	0.	0.
TOTAL		2.411E-09	7.074E-09	2.406E-09	1.655E-09	1.833E-09

****

TABLE I. (CONTINUED)

POLAR ANGLE		7.500E+01	7.500E+01	9.000E+01	9.000E+01	9.000E+01
		9.000E+01	9.000E+01	1.200E+02	1.200E+02	1.200E+02
AZIMUTHAL ANGLE		9.000E+01	1.350E+02	0.	1.125E+01	2.250E+01
		1.350E+02	1.800E+02	1.125E+01	2.250E+01	4.500E+01
TIME INTERVAL						
*********	-1.000E-07	0.	0.	0.	0.	0.
1.000E-07	-1.500E-07	0.	0.	0.	0.	0.
1.500E-07	-2.000E-07	0.	0.	0.	0.	0.
2.000E-07	-2.500E-07	0.	0.	0.	0.	0.
2.500E-07	-3.000E-07	2.187E-10	0.	3.528E-10	0.	0.
3.000E-07	-4.000E-07	9.254E-12	3.982E-11	0.	0.	5.351E-11
4.000E-07	-5.000E-07	1.500E-12	3.557E-12	0.	9.858E-12	0.
5.000E-07	-6.000E-07	1.433E-10	5.442E-13	2.687E-11	8.220E-11	1.283E-11
6.000E-07	-8.000E-07	3.184E-11	7.079E-11	5.446E-12	6.884E-11	5.544E-10
8.000E-07	-1.000E-06	6.879E-11	7.735E-12	2.914E-11	6.393E-11	2.399E-10
1.000E-06	-1.500E-06	8.971E-10	1.119E-09	1.142E-10	5.445E-11	8.340E-11
1.500E-06	-2.000E-06	3.116E-10	2.014E-09	8.543E-11	2.550E-11	1.140E-10
2.000E-06	-2.500E-06	8.468E-10	1.152E-11	8.424E-11	5.363E-11	3.823E-10
2.500E-06	-3.000E-06	5.443E-11	2.945E-10	1.145E-11	1.150E-11	7.601E-12
3.000E-06	-4.000E-06	2.846E-11	2.827E-11	2.366E-10	4.293E-11	1.075E-09
4.000E-06	-5.000E-06	1.780E-11	3.273E-10	4.798E-11	6.354E-10	1.803E-11
5.000E-06	-6.000E-06	2.814E-11	1.324E-09	4.325E-13	1.130E-12	3.598E-11
6.000E-06	-8.000E-06	2.370E-11	4.246E-09	4.621E-12	9.232E-12	1.955E-10
8.000E-06	-1.000E-05	3.844E-11	6.881E-11	2.035E-11	7.240E-12	1.663E-11
1.000E-05	-1.500E-05	1.572E-23	2.492E-29	4.448E-29	3.947E-31	9.658E-30
1.500E-05	-2.000E-05	0.	0.	0.	0.	0.
2.000E-05	-2.500E-05	0.	0.	0.	0.	0.
2.500E-05	-3.000E-05	0.	0.	0.	0.	0.
3.000E-05	-4.000E-05	0.	0.	0.	0.	0.
4.000E-05	-5.000E-05	0.	0.	0.	0.	0.
5.000E-05	-6.000E-05	0.	0.	0.	0.	0.
6.000E-05	-8.000E-05	0.	0.	0.	0.	0.
8.000E-05	-1.000E-04	0.	0.	0.	0.	0.
1.000E-04	-1.500E-04	0.	0.	0.	0.	0.
1.500E-04	-2.000E-04	0.	0.	0.	0.	0.
2.000E-04	-2.500E-04	0.	0.	0.	0.	0.
2.500E-04	-3.000E-04	0.	0.	0.	0.	0.
3.000E-04	-4.000E-04	0.	0.	0.	0.	0.
4.000E-04	-5.000E-04	0.	0.	0.	0.	0.
5.000E-04	-6.000E-04	0.	0.	0.	0.	0.
6.000E-04	-8.000E-04	0.	0.	0.	0.	0.
8.000E-04	-1.000E-03	0.	0.	0.	0.	0.
TOTAL		2.720E-09	9.556E-09	1.020E-09	1.072E-09	2.794E-09

****

TABLE I. (CONTINUED)

POLAR ANGLE		9.000E+01	9.000E+01	9.000E+01	1.200E+02	1.200E+02
		1.200E+02	1.200E+02	1.200E+02	1.500E+02	1.500E+02
AZIMUTHAL ANGLE		4.500E+01	9.000E+01	1.350E+02	0.	1.125E+01
		9.000E+01	1.350E+02	1.800E+02	1.125E+01	2.250E+01
TIME INTERVAL						
*********	-1.000E-07	0.	0.	0.	0.	0.
1.000E-07	-1.500E-07	0.	0.	0.	0.	0.
1.500E-07	-2.000E-07	0.	0.	0.	0.	0.
2.000E-07	-2.500E-07	0.	0.	0.	0.	0.
2.500E-07	-3.000E-07	1.673E-11	5.738E-11	0.	0.	0.
3.000E-07	-4.000E-07	0.	0.	0.	0.	2.011E-10
4.000E-07	-5.000E-07	0.	1.005E-10	1.316E-11	0.	0.
5.000E-07	-6.000E-07	3.324E-11	8.907E-11	1.991E-10	0.	6.783E-11
6.000E-07	-8.000E-07	1.085E-10	5.040E-10	4.775E-11	8.412E-12	4.440E-11
8.000E-07	-1.000E-06	9.321E-10	1.096E-11	7.649E-11	4.836E-11	3.331E-11
1.000E-06	-1.500E-06	2.025E-09	3.408E-10	1.604E-09	7.433E-11	3.731E-12
1.500E-06	-2.000E-06	2.798E-10	1.145E-10	2.532E-10	3.099E-11	1.458E-11
2.000E-06	-2.500E-06	4.810E-10	4.305E-11	4.961E-10	1.244E-11	9.083E-12
2.500E-06	-3.000E-06	2.190E-11	5.474E-11	1.609E-10	1.124E-11	1.146E-11
3.000E-06	-4.000E-06	3.294E-10	1.716E-10	2.160E-10	1.170E-10	1.299E-10
4.000E-06	-5.000E-06	7.990E-11	2.214E-10	2.254E-10	3.732E-12	3.786E-12
5.000E-06	-6.000E-06	8.999E-09	5.104E-11	8.291E-11	1.490E-11	5.098E-11
6.000E-06	-8.000E-06	6.490E-10	1.973E-09	9.747E-10	1.749E-10	6.051E-10
8.000E-06	-1.000E-05	5.392E-10	7.475E-10	4.845E-10	2.942E-11	1.255E-11
1.000E-05	-1.500E-05	1.635E-29	8.682E-31	2.377E-28	1.220E-28	9.459E-33
1.500E-05	-2.000E-05	0.	0.	0.	0.	0.
2.000E-05	-2.500E-05	0.	0.	0.	0.	0.
2.500E-05	-3.000E-05	0.	0.	0.	0.	0.
3.000E-05	-4.000E-05	0.	0.	0.	0.	0.
4.000E-05	-5.000E-05	0.	0.	0.	0.	0.
5.000E-05	-6.000E-05	0.	0.	0.	0.	0.
6.000E-05	-8.000E-05	0.	0.	0.	0.	0.
8.000E-05	-1.000E-04	0.	0.	0.	0.	0.
1.000E-04	-1.500E-04	0.	0.	0.	0.	0.
1.500E-04	-2.000E-04	0.	0.	0.	0.	0.
2.000E-04	-2.500E-04	0.	0.	0.	0.	0.
2.500E-04	-3.000E-04	0.	0.	0.	0.	0.
3.000E-04	-4.000E-04	0.	0.	0.	0.	0.
4.000E-04	-5.000E-04	0.	0.	0.	0.	0.
5.000E-04	-6.000E-04	0.	0.	0.	0.	0.
6.000E-04	-8.000E-04	0.	0.	0.	0.	0.
8.000E-04	-1.000E-03	0.	0.	0.	0.	0.
TOTAL		1.450E-08	4.484E-09	4.834E-09	5.262E-10	1.188E-09

****

TABLE I. (CONTINUED)

POLAR ANGLE		1.200E+02	1.200E+02	1.200E+02	1.200E+02	1.500E+02
		1.500E+02	1.500E+02	1.500E+02	1.500E+02	1.800E+02
AZIMUTHAL ANGLE		2.250E+01	4.500E+01	9.000E+01	1.350E+02	0.
		4.500E+01	9.000E+01	1.350E+02	1.800E+02	1.125E+01
TIME INTERVAL						
*********	-1.000E-07	0.	0.	0.	0.	0.
1.000E-07	-1.500E-07	0.	0.	0.	0.	0.
1.500E-07	-2.000E-07	0.	0.	0.	0.	0.
2.000E-07	-2.500E-07	0.	0.	0.	0.	0.
2.500E-07	-3.000E-07	0.	0.	0.	0.	0.
3.000E-07	-4.000E-07	3.713E-10	0.	8.113E-11	0.	0.
4.000E-07	-5.000E-07	0.	0.	0.	0.	0.
5.000E-07	-6.000E-07	1.521E-10	8.880E-11	1.872E-10	0.	0.
6.000E-07	-8.000E-07	2.611E-11	8.537E-11	1.152E-10	2.389E-10	0.
8.000E-07	-1.000E-06	8.142E-12	3.315E-10	9.571E-10	1.234E-10	7.105E-12
1.000E-06	-1.500E-06	6.349E-11	1.603E-0	6.887E-10	3.632E-10	5.866E-12
1.500E-06	-2.000E-06	6.394E-10	1.590E-10	1.032E-10	5.422E-11	2.416E-12
2.000E-06	-2.500E-06	1.832E-10	1.998E-0	2.468E-09	1.047E-10	9.679E-11
2.500E-06	-3.000E-06	2.566E-12	2.758E-11	4.209E-11	6.685E-12	9.250E-12
3.000E-06	-4.000E-06	2.289E-11	4.012E-10	2.324E-10	1.799E-10	5.233E-12
4.000E-06	-5.000E-06	3.271E-09	9.309E-11	3.718E-10	4.770E-10	8.432E-13
5.000E-06	-6.000E-06	1.387E-10	3.356E-11	5.813E-11	3.791E-11	8.074E-11
6.000E-06	-8.000E-06	1.155E-10	1.550E-10	2.266E-10	2.693E-11	5.106E-11
8.000E-06	-1.000E-05	3.726E-12	2.125E-11	2.398E-10	4.990E-10	9.955E-13
1.000E-05	-1.500E-05	9.276E-32	5.190E-30	3.455E-30	4.031E-26	0.
1.500E-05	-2.000E-05	0.	0.	0.	0.	0.
2.000E-05	-2.500E-05	0.	0.	0.	0.	0.
2.500E-05	-3.000E-05	0.	0.	0.	0.	0.
3.000E-05	-4.000E-05	0.	0.	0.	0.	0.
4.000E-05	-5.000E-05	0.	0.	0.	0.	0.
5.000E-05	-6.000E-05	0.	0.	0.	0.	0.
6.000E-05	-8.000E-05	0.	0.	0.	0.	0.
8.000E-05	-1.000E-04	0.	0.	0.	0.	0.
1.000E-04	-1.500E-04	0.	0.	0.	0.	0.
1.500E-04	-2.000E-04	0.	0.	0.	0.	0.
2.000E-04	-2.500E-04	0.	0.	0.	0.	0.
2.500E-04	-3.000E-04	0.	0.	0.	0.	0.
3.000E-04	-4.000E-04	0.	0.	0.	0.	0.
4.000E-04	-5.000E-04	0.	0.	0.	0.	0.
5.000E-04	-6.000E-04	0.	0.	0.	0.	0.
6.000E-04	-8.000E-04	0.	0.	0.	0.	0.
8.000E-04	-1.000E-03	0.	0.	0.	0.	0.
TOTAL		4.998E-09	4.997E-09	5.782E-09	2.117E-09	2.613E-10

****

TABLE I. (CONTINUED)

POLAR ANGLE		1.500E+02	1.500E+02	1.500E+02	1.500E+02	1.500E+02
		1.800E+02	1.800E+02	1.800E+02	1.800E+02	1.800E+02
AZIMUTHAL ANGLE		1.125E+01	2.250E+01	4.500E+01	9.000E+01	1.350E+02
		2.250E+01	4.500E+01	9.000E+01	1.350E+02	1.800E+02
TIME INTERVAL						
*********	-1.000E-07	0.	0.	0.	0.	0.
1.000E-07	-1.500E-07	0.	0.	0.	0.	0.
1.500E-07	-2.000E-07	0.	0.	0.	0.	0.
2.000E-07	-2.500E-07	0.	0.	0.	0.	0.
2.500E-07	-3.000E-07	0.	0.	0.	0.	0.
3.000E-07	-4.000E-07	0.	0.	0.	0.	0.
4.000E-07	-5.000E-07	0.	0.	0.	0.	0.
5.000E-07	-6.000E-07	0.	0.	2.114E-10	0.	0.
6.000E-07	-8.000E-07	0.	0.	4.909E-10	6.261E-11	2.439E-10
8.000E-07	-1.000E-06	0.	1.217E-10	2.366E-11	6.527E-11	0.
1.000E-06	-1.500E-06	1.997E-11	2.542E-11	3.137E-11	1.051E-10	9.412E-10
1.500E-06	-2.000E-06	2.881E-12	2.478E-11	8.279E-12	1.372E-11	1.923E-11
2.000E-06	-2.500E-06	2.310E-12	7.511E-11	5.228E-12	2.192E-11	2.125E-11
2.500E-06	-3.000E-06	1.546E-11	1.763E-11	9.731E-12	1.569E-12	2.579E-12
3.000E-06	-4.000E-06	1.351E-11	1.360E-11	2.257E-11	1.350E-11	8.467E-12
4.000E-06	-5.000E-06	2.355E-11	5.374E-10	1.096E-10	9.618E-12	5.027E-10
5.000E-06	-6.000E-06	4.194E-12	1.849E-11	1.311E-11	1.437E-12	2.310E-12
6.000E-06	-8.000E-06	4.363E-12	2.211E-12	1.560E-10	3.050E-10	2.260E-11
8.000E-06	-1.000E-05	4.086E-13	7.914E-12	1.060E-11	1.605E-11	2.108E-11
1.000E-05	-1.500E-05	0.	0.	4.845E-32	2.132E-33	2.169E-27
1.500E-05	-2.000E-05	0.	0.	0.	0.	0.
2.000E-05	-2.500E-05	0.	0.	0.	0.	0.
2.500E-05	-3.000E-05	0.	0.	0.	0.	0.
3.000E-05	-4.000E-05	0.	0.	0.	0.	0.
4.000E-05	-5.000E-05	0.	0.	0.	0.	0.
5.000E-05	-6.000E-05	0.	0.	0.	0.	0.
6.000E-05	-8.000E-05	0.	0.	0.	0.	0.
8.000E-05	-1.000E-04	0.	0.	0.	0.	0.
1.000E-04	-1.500E-04	0.	0.	0.	0.	0.
1.500E-04	-2.000E-04	0.	0.	0.	0.	0.
2.000E-04	-2.500E-04	0.	0.	0.	0.	0.
2.500E-04	-3.000E-04	0.	0.	0.	0.	0.
3.000E-04	-4.000E-04	0.	0.	0.	0.	0.
4.000E-04	-5.000E-04	0.	0.	0.	0.	0.
5.000E-04	-6.000E-04	0.	0.	0.	0.	0.
6.000E-04	-8.000E-04	0.	0.	0.	0.	0.
8.000E-04	-1.000E-03	0.	0.	0.	0.	0.
TOTAL		8.715E-11	8.453E-10	1.103E-09	6.158E-10	1.785E-09

****

THART-L calculations were also made for a source rotated 60 and 90 degrees from the source-receiver axis in addition to the computation for the source rotated 30 degrees from the source-receiver axis. The time integrated results received within each solid angle interval was divided by the size of the solid angle and these results, the number of photons per square meter per steradian entering the reciever within each of the solid angle intervals for each photon emitted from the source, are listed in Tables II, III, and IV. It is extremely difficult to determine any trends in the angular distributions of the scattered intensities due to the large fluctuations in the data, thus no attempt was made to curve fit the data or extrapolate these data to other source directions. Instead the method used to apply these results to predict the time distribution of the signal observed by a satellite due to a point source beneath a cloud used the actual data from the THART-L program.

Prior to discussing that method, the TPART-III calculations as discussed earlier are presented and compared with those from THART-L. Table V shows the time integrated response computed with the TPART-III program for the collimated receiver located at 765 meters from the laser source where both the source and receiver are within a cloud. The TPART-III calculations modeled the telescope receiver used for Project CLIPS which had an outside diameter of 14 inches and the central portion of the field of view blocked by a 4.5 inch diameter secondary mirror. The calculations modeled the telescope operated with a 1 degree field of view, thus the time integrated receiver response is the number of photons crossing the detection area of the telescope within a 1 degree field of view for each photon emitted from the source. To convert these data to photons per square meter per steradian the response was divided by the area of the telescope detection area and the solid angle of the 1 degree field of view. These data are shown in the right hand column of Table V. Note the sharp peak when the source and receiver point directly toward each other. As both the source and receiver are moved off axis, the response drops 4 to 5 orders of

TABLE II. ANGULAR DISTRIBUTION OF THE TIME INTEGRATED IRRADIANCE FOR A MONODIRECTIONAL SOURCE ROTATED 30 DEGREES FROM THE SOURCE-RECEIVER AXIS

Polar Angle (deg)	Azimuthal Angle (deg)					
	0-11.25	11.25-22.5	22.5-45.0	45-90	90-135	135-180
0-10	5.109-8	1.208-7	1.548-7	7.851-8	8.691-8	1.918-7
10-20	5.611-8	3.293-7	6.107-7	4.967-7	6.285-8	4.683-7
20-30	4.137-8	4.772-8	9.058-8	5.692-7	1.294-7	3.096-8
30-45	3.672-8	8.634-8	4.376-8	6.923-8	4.936-8	2.983-9
45-60	1.028-6	1.244-8	4.552-8	4.693-8	1.553-8	6.172-8
60-75	2.920-8	1.815-8	2.169-8	1.219-8	1.564-8	1.273-8
75-90	1.392-7	4.734-8	1.628-8	9.263-9	1.338-8	4.701-8
90-120	1.039-8	1.092-8	1.423-8	3.692-8	1.142-8	1.231-8
120-150	7.322-9	1.653-8	3.477-8	1.738-8	2.011-8	7.364-9
150-180	9.933-9	3.313-9	1.607-8	1.048-8	5.852-9	1.696-8

TABLE III. ANGULAR DISTRIBUTION OF THE TIME INTEGRATED IRRADIANCE FOR A MONODIRECTIONAL SOURCE ROTATED 60 DEGREES FROM THE SOURCE-RECEIVER AXIS

Polar Angle (deg)	Azimuthal Angle (deg)					
	0-11.25	11.25-22.5	22.5-45.0	45-90	90-135	135-180
0-10	3.393-9	7.382-9	2.159-8	1.312-9	2.324-9	3.440-8
10-20	6.176-8	2.735-8	5.599-9	1.099-8	8.723-9	7.719-9
20-30	2.611-8	2.716-8	1.031-7	3.208-8	8.953-7	3.104-8
30-45	5.977-9	8.630-8	7.153-8	3/037-8	8.292-8	3.625-8
45-60	1.359-9	1.117-7	1.066-8	4.149-9	1.550-9	1.069-9
60-75	2.988-9	3.202-8	1.350-8	6.476-9	3.157-9	3.328-9
75-90	3.109-9	2.597-9	5.618-8	1.748-9	4.773-7	1.289-7
90-120	3.355-8	7.733-9	1.317-8	9.717-9	2.313-8	1.641-8
120-150	1.123-8	1.240-7	4.833-7	9.274-8	2.315-9	6.168-9
150-180	1.785-9	3.167-9	2.026-8	1.203-8	3.810-9	2.538-8

TABLE IV. ANGULAR DISTRIBUTION OF THE TIME INTEGRATED IRRADIANCE FOR A MONODIRECTIONAL SOURCE ROTATED 90 DEGREES FROM THE SOURCE-RECEIVER AXIS

Polar Angle (deg)	Azimuthal Angle (deg)					
	0-11.25	11.25-22.5	22.5-45.0	45-90	90-135	135-180
0-10	3.550-9	2.862-7	6.876-9	2.430-6	7.839-7	8.202-8
10-20	6.579-8	4.641-9	8.032-8	6.516-9	5.464-8	2.064-9
20-30	1.647-5	5.008-9	2.301-8	3.462-9	5.016-9	1.886-7
30-45	1.029-8	1.439-8	2.267-8	1.385-8	5.961-9	4.570-9
45-60	1.032-8	4.038-9	3.220-9	1.415-8	3.799-9	2.598-9
60-75	2.996-9	3.341-9	3.584-9	1.559-9	2.414-9	3.812-9
75-90	3.975-8	3.268-9	3.033-8	7.005-9	2.087-9	1.540-9
90-120	7.700-9	2.571-9	6.600-8	1.621-8	7.927-9	2.207-9
120-150	4.428-9	1.269-9	1.320-7	1.466-9	3.200-8	1.968-9
150-180	1.816-10	4.151-10	4.870-10	3.677-9	8.317-10	2.435-10

TABLE V. TIME INTEGRATED RESPONSES CALCULATED WITH THE TPART-III PROGRAM

Source Direction	Receiver Direction	Telescope Response	Photon M^2-ster
0	0	3.1-08	1.46-3
	1	9.0-09	4.22-4
	2	6.1-11	2.86-6
	3	4.5-11	2.11-6
	5	4.9-11	2.30-6
	10	2.8-11	1.31-6
5	0	8.5-11	3.99-6
	1	6.2-11	2.91-6
	2	8.1-11	3.80-6
	3	2.3-11	1.08-6
	5	2.8-11	1.31-6
	10	2.0-11	9.39-7
10	0	8.2-12	3.85-7
	1	5.2-12	2.44-7
	2	4.9-12	2.30-7
	3	8.4-12	3.94-7
	5	1.6-11	7.51-7
	10	7.3-12	3.43-7
15	5	4.74-12	3.43-7
	10	5.68-12	2.66-7
	15	7.27-12	3.41-7
	20	2.93-12	1.38-7
	30	1.93-12	9.06-8
20	10	3.00-12	1.41-7
	15	1.19-11	5.59-7
	20	4.25-12	2.00-7
30	5	3.00-12	1.78-7
	10	2.80-12	1.31-7
	15	5.07-12	2.38-7
	20	2.10-12	9.86-8
	30	1.20-12	5.63-8

of magnitude and tends to flatten out. Note also that the time integrated intensities for the source oriented 30 degrees off axis are of the same order of magnitude as the time integrated intensities computed with the THART-L program.

III. MODELING POINT SOURCE BENEATH CLOUD WITH NARROW-BEAM TRANSMISSION DATA

Although the statistical fluctuations in the intensities computed as a function of time and direction with the TPART-III and THART-L programs for the source scanned at the different angles were extremely poor, these data have been used to predict the time dependent intensity at a satellite receiver due to a point source located at the center of a dome shaped cloud which has a 765 meter geometric radius and an optical radius of 14.7.

First the number of photons, $I(\Delta\theta_i,\Delta\phi_j,\Delta t_k,\theta_{o\ell})$, calculated with the THART-L program for the polar angle interval $\Delta\theta_i$, azimuthal angle interval $\Delta\phi_j$, and time interval Δt_k were divided by the solid angle interval $\Delta\phi_j\Delta\cos\theta_i$, and the time interval Δt_k, to obtain the number of photons per square meter per steradian per second in the direction, (θ,ϕ) for a source emitted in the direction $\theta_{o\ell}$. These data were then weighted with a source solid angle interval $\frac{\Delta\cos\theta_{o\ell}}{2\pi} * \frac{\Delta\phi_j}{2\pi}$ and summed over ϕ and θ_o to give the intensity per steradian in the direction polar θ_i,

$$N(\Delta\theta_i,\ \Delta t_k) = \sum_{\Delta\cos\theta_{o\ell}} \sum_{\Delta\phi_j} \frac{I(\Delta\theta_i,\ \Delta\phi_\Delta, t_k, \phi_{o\ell})}{\Delta\phi_j * \Delta\cos\theta_i * \Delta t_k} * \frac{\Delta\phi_j}{2\pi} * \frac{\Delta\cos\theta_{o\ell}}{2},$$

for an isotropic source located a distance of 765 meters from the source. It was assumed that this intensity actually determined for a receiver embedded within a cloud was the intensity per steradian per second leaking from all points on the surface of a dome shaped cloud. The intensity leaking from a point on the surface of the cloud that would reach a synchronous satellite at a distance of 35800 kilometers away would be $N(\Delta\theta_i,\Delta t_k)/35800^2$. For the satellite stationed directly above this dome shaped cloud, and for a unit area located at an angle θ_i from the radial through the receiver position the emission from the surface that would intersect the satellite receiver would also be in a direction θ_i from the normal to the surface. Therefore multiplying $N(\Delta\theta_i,\Delta t_k)/35800^2$

by $2\pi \cdot 765^2 \cdot \Delta\cos\theta_i$ and summing over all surface areas gives the time dependent intensity in units of photons/km^2-sec at a satellite receiver.

The calculation as discussed above was performed using the THART-L results for 30, 60 and 90 degree source directions to represent the emission from an isotropic source in the source polar angle intervals 0-45, 45-75, and 75-180 degrees, respectively, The time distributions of the scattered intensity computed using the THART-L results are shown in Figure 9.

Although the THART-L calculations agreed reasonably well with the TPART-III program for the 30 degree off axis source direction, it is anticipated that the assumption that the 30 degree source direction was representative of the sources directed more toward the receiver may not have been too accurate. Thus it was decided to add the TPART-III results for a source emitting radiation out to 17.5 degrees integrating over that portion of the cloud surface corresponding to the maximum receiver angles used in the TPART-III calculations. Although the TPART-III calculations were all made with the source and receiver scanned off axis in the same azimuthal plane it was assumed that the response at all azimuthal angles would be the same as that in the source azimuthal plane. The TPART-III results computed for the source pointed directly toward the receiver position were used to represent the emission from a point source out to 2.5 degrees. The TPART-III results for a source angle scanned 5 degrees off the source-receiver axis was used to represent the emission from a point source between the polar angles of 2.5 and 7.5 degrees and etc. Thus the TPART-III results for each source direction, ℓ, was multiplied by the source solid angle, $2\pi\Delta\cos\theta_{o\ell}$, and then the intensity within each receiver direction, i, was multiplied by the area $765^2 * 2\pi\Delta\cos\theta_i$, on the surface of the dome shaped cloud from which the direction of emission toward the satellite receiver is θ_i. These values were divided by the square of the distance from the cloud top to the satellite receiver position to give the time dependent intensity at the satellite receiver,

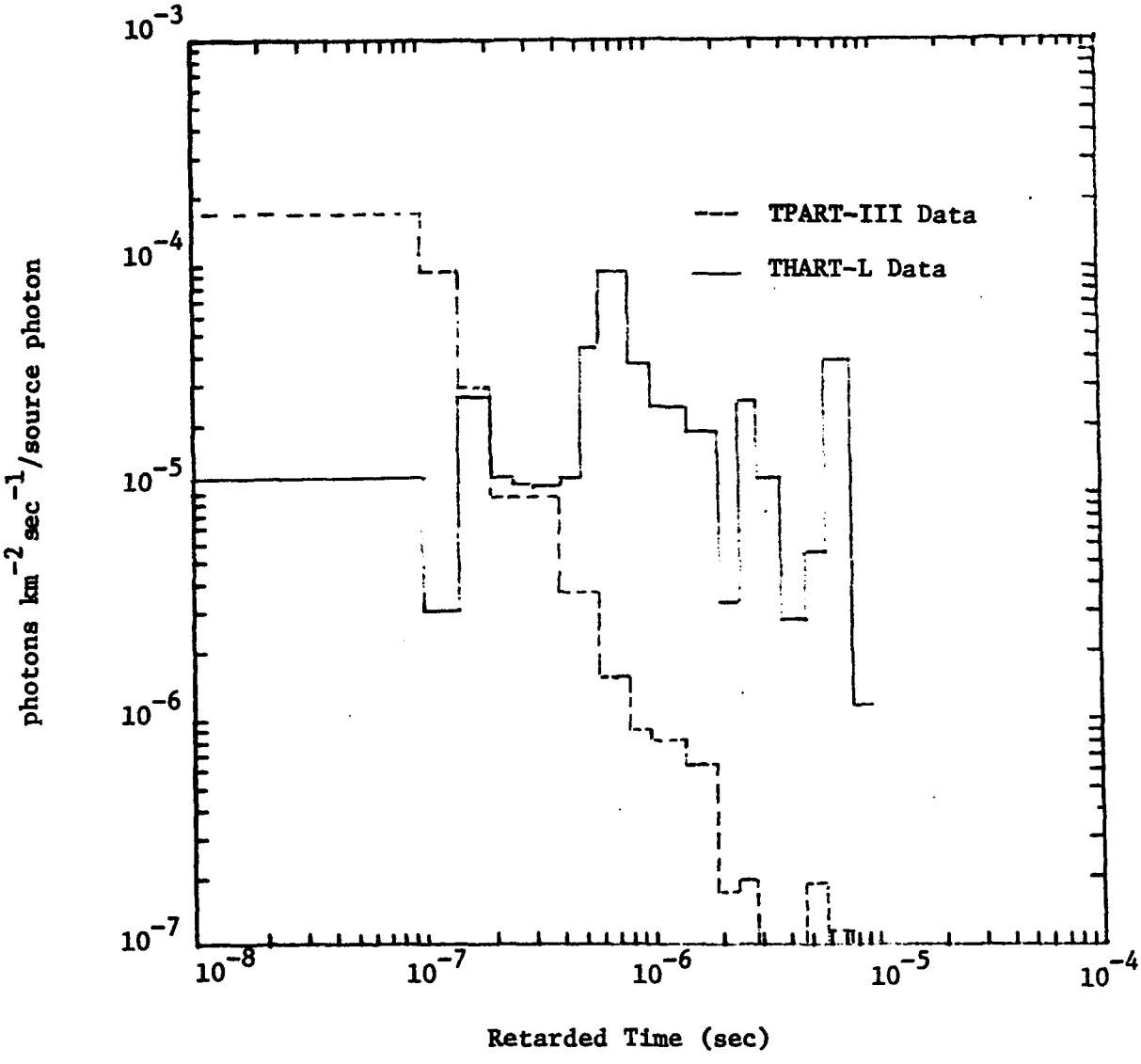

Fig. 9. Time Distributions of the Irradiance for a Synchronous Satellite Above a Dome Shaped Cloud. Calculated Using Narrow Beam Source-Receiver Transmission Data

$$R(\Delta t_k) = \sum_{\Delta\theta} \sum_{\Delta\theta_o} T(\theta_{o\ell}, \Delta\theta_i, \Delta t_k) * 2\pi\Delta\cos\theta_{o\ell} * 765^2 * 2\pi\Delta\cos\theta_i / 35800^2 ,$$

where $T(\theta_{o\ell}, \Delta\theta_i, \Delta t_k)$ is the TPART-III response normalized to give the number of photons per second per square meter per steradian. The time dependent satellite response computed using the TPART-III results are shown in Figure 9, along with that computed using the THART-L data. The response computed using the TPART-III data is initially higher than the response computed using the THART-L data but quickly decays because the TPART-III data did not include the source emitted at large angles and the emission was not integrated over the entire surface of the dome shaped cloud. The response computed using the THART-L data is thought to be the more realistic response for the later time since that response was computed using narrow beam transmission data representing the emission in 4π steradian about the source and the integration of the emission over the surface of the dome shaped cloud was complete.

The two responses computed using the narrow beam data were summed together and this sum is compared with a satellite receiver response computed with the POLOE program, see Figure 10. The cloud model used in the POLOE calculation was a 1530 meter thick cloud layer adjacent to the ground surface with no atmosphere above or below the cloud. The scattering and attenuating properties of the cloud was the same as those used in defining the clouds for the narrow-beam transmission calculations. A 532 nanometer wavelength point isotropic source was located at mid altitude in the cloud which is 765 meters below the upper surface and at an optical depth of 14.7, the same as the source-receiver optical separation distance in the narrow beam calculations. The time dependent response was computed for a synchronous satellite located 35,800 kilometers above the cloud top.

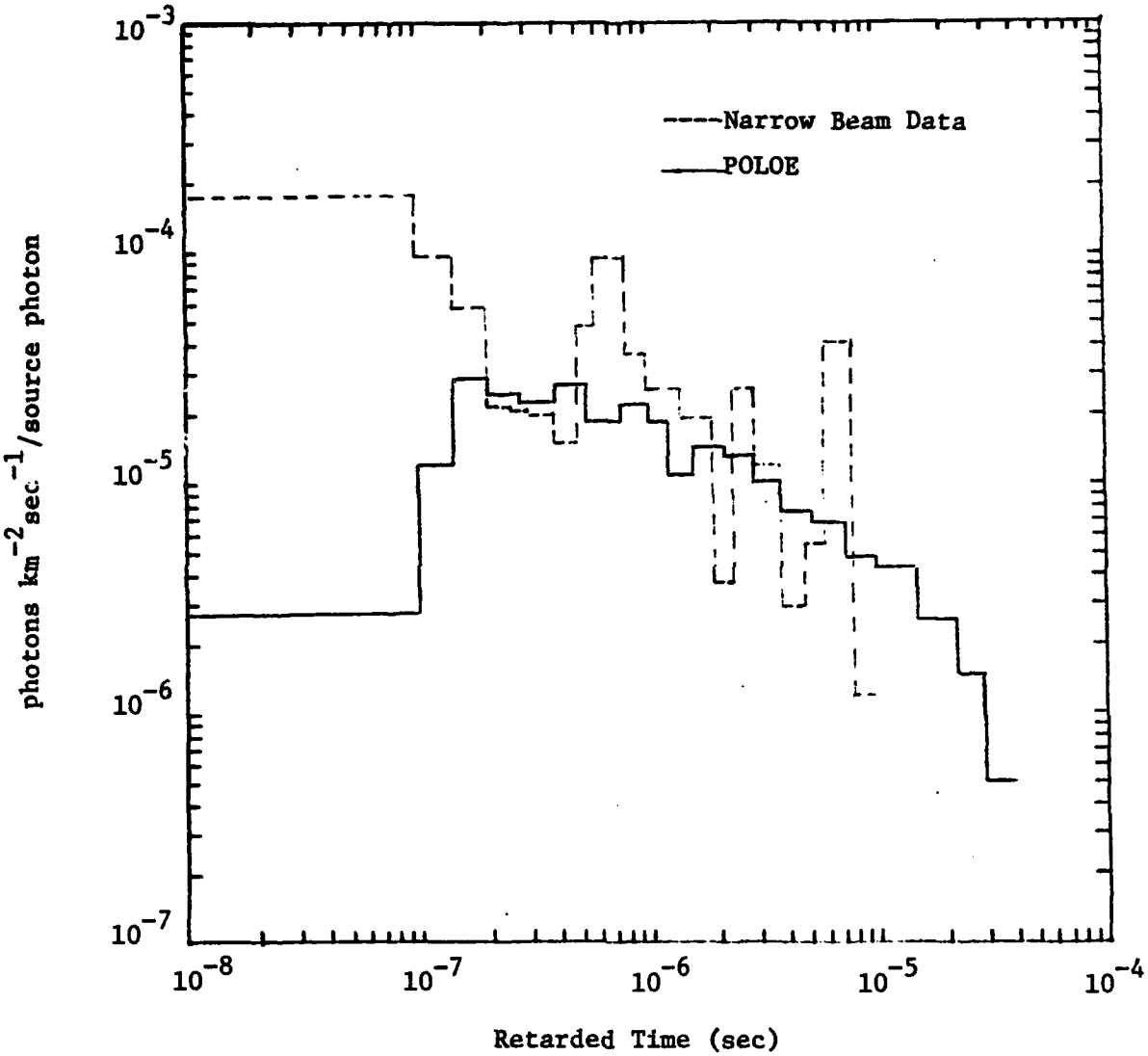

Fig. 10. Comparisons of Time Dependent Synchronous Satellite Response Computed Using Narrow Beam Source Receiver Data with the Response Computed Using the POLOE Program

The responses computed using the narrow-beam data and with the POLOE program are in extremely good agreement beyond a few tenths of a microsecond, especially since the response for the narrow-beam data is for a dome shaped cloud and the POLOE response is for a cloud layer. The comparison still leaves some question about the early time response. These differences cannot be attributed to the differences in the cloud shape because the early time response has been determined to come from the cloud surface just above the source position. It is in this region that the cloud geometries are most similiar. It is recalled that the peak during the early time of the response calculated using the narrow beam data was due to the inclusion of the TPART-III calculations. Since the decrease in the narrow-beam transmission with increasing angle as the source was scanned off the source-receiver axis was so rapid, the solid angle intervals selected to be represented by each of the source directions would have an affect on the magnitude of the combined results. In addition the assumption that the same response would be observed from all azimuthal directions as was observed from within the source azimuth plane would also tend to cause the response to be higher during early times. Under these circumstances it concluded that there is really no significant inconsistancies in the time distributions computed for narrow-beam source receiver geometries and for satellite observations of a point source beneath a cloud.

REFERENCES

1. D. G. Collins, J. M. Newell, D. M. Brown, R. B. Livesay, and M. B. Wells, Monte Carlo Studies of Air Fluorescence, Thermal Radiation and Nuclear Radiation Transport in the Atmosphere, Radiation Research Association, Inc. Report RRA T-7815 (April 1979)

2. D. G. Collins, Time Delay and Pulse Stretching Calculations for Laser Radiation Propagation in Clouds, Radiation Research Association, Inc. Report RRA-T7905 (April 1979)

DISTRIBUTION LIST

Lt. Col. M. Schneider AFTAC/TFS	5 copies
Maj. C. Menelly ATTAC/TFR	2 copies
J. S. Williams Sandia Laboratories Div. 1241	3 copies